

**ALMA MATER STUDIORUM - UNIVERSITÀ DI BOLOGNA**

---

**SCUOLA DI INGEGNERIA E ARCHITETTURA**

*DIPARTIMENTO DI INGEGNERIA DELL'ENERGIA ELETTRICA E  
DELL'INFORMAZIONE G. MARCONI*

*CORSO DI LAUREA MAGISTRALE IN INGEGNERIA ENERGETICA*

**TESI DI LAUREA MAGISTRALE**

In

Tecnologie Innovative per la Produzione, il Trasporto e l'Accumulo  
dell'Energia Elettrica M

**Surface Plasmon Induced Luminescence as a Tool for Study of  
the Ageing of Polymeric Materials**

CANDIDATO

Luca Montanari

RELATORE:

Prof. Ing. Davide Fabiani

CORRELATORI:

Dr. Gilbert Teyssedre  
Dr. Kremena Makasheva  
Dr. Christian Laurent

Anno Accademico 2015/16

Sessione III



# Table of Contents

<b>Chapter 1 State of the Art</b> .....	5
<b>1.1 Insulating polymers and electrical applications</b> .....	5
1.1.1 Polymeric materials: from insulators to conductors.....	5
1.1.2 A Brief History of Development in Electrical Insulation .....	7
a) From oil impregnated paper to Polyethylene.....	7
b) Composites and nanocomposites.....	9
<b>1.2 Reliability of insulating materials</b> .....	10
1.2.1 Key properties of insulating materials .....	10
1.2.2 Space charge as a threat in insulating polymers .....	11
1.2.3 Ageing Diagnosis.....	12
<b>1.3 Luminescence processes in insulating polymers</b> .....	13
1.3.1 Introduction .....	13
1.3.2 Photoluminescence – optical excitation .....	15
a) Fluorescence.....	15
b) Phosphorescence.....	16
1.3.3 Electroluminescence.....	17
a) Electroluminescence mechanism in dielectric materials.....	18
b) Relaxation process and possible luminescent centres .....	19
c) Electroluminescence and electrical ageing .....	20
<b>1.4 Surface Plasmons</b> .....	22
1.4.1 Introduction.....	22
1.4.2 Coupling surface plasmons and photons: conditions for radiate relaxation.....	23
1.4.3 Spectral distribution of the light emitted by SP.....	24
1.4.4 SP implication in electroluminescence spectra.....	25
1.4.5 Silver nanoparticles (AgNPs) as the most appropriate nanostructures to support surface plasmons.....	26
<b>1.5 Purpose of the thesis</b> .....	29
<b>1.6 Plasma deposition techniques for synthesis of AgNPs in silica-like matrix</b> .....	32

1.6.1	Introduction.....	32
1.6.2	Plasma Enhanced Chemical Vapor Deposition (PECVD) .....	33
<b>Chapter 2 Experimental Materials and Techniques</b> .....		<b>35</b>
<b>2.1</b>	<b>Materials (Polypropylene)</b> .....	<b>35</b>
<b>2.2</b>	<b>Experimental setups</b> .....	<b>36</b>
2.2.1	Sample preparation .....	37
a)	Gold metallization setup .....	37
b)	ITO sputtering setup.....	37
c)	Treatment of electrode edges.....	38
2.2.2	Luminescence setup.....	39
a)	Excitation source .....	40
b)	The photomultiplier detector – photons counting .....	44
c)	The monochromator and CCD camera – spectra acquisition.....	44
2.2.3	Plasma reactor description .....	45
2.2.4	Monitoring of the plasma process by OES .....	49
2.2.5	Ellipsometry.....	50
<b>Chapter 3 Experimental results</b> .....		<b>53</b>
Synopsis .....		53
<b>3.1</b>	<b>EL from reference structures</b> .....	<b>53</b>
3.1.1	Samples .....	53
3.1.2	Protocols .....	55
3.1.3	Field dependence of EL under AC stress .....	59
3.1.4	Phase resolved EL under AC stress.....	62
3.1.5	Discussion .....	68
<b>3.2</b>	<b>AgNPs tailored BOPP: structure and EL characterisation</b> .....	<b>72</b>
3.2.1	Sample preparation .....	73
3.2.2	Physico-chemical characterization of the composite layer .....	75
3.2.3	Field dependence of EL under AC stress .....	78
3.2.4	Spectral analyses .....	84
3.2.5	Discussion .....	86
<b>3.3</b>	<b>Conclusion and Perspective</b> .....	<b>89</b>
References .....		92





# Chapter 1 State of the Art

## 1.1 Insulating polymers and electrical applications

Polymers are frequently found in our surroundings from personal computers to car manufacturing, from living facilities to military installations. More specifically, some insulating polymers are widely used with their electrical insulating properties to electrical engineering applications.

The term polymer has been used since the early 1830s and was first coined by Jons Jakob Berzelius [1]. However, a true understanding was not attained until the 1920s and, since then, some of the most famous polymers have been developed, such as – Nylon, polyethylene, Teflon and silicones [2].

A polymer is composed of a long chain of repeated units, called monomers. The most common technological polymers are plastics, issued from petroleum industry, however there are other forms such as cellulose, a naturally occurring polymer found in plants. Engineering plastics can be created from a single polymer, or by adding a second phase, e.g. an inorganic materials to form a composite. In this way it is possible to enhance key properties to render the base polymer more suitable for use in a particular application.

Specially, polymers have a very important role as insulating media because of their electrical and thermal properties. Furthermore polymers are usually easy to produce and they have a low effective cost. Polymers are often manufactured for strengthened properties, for example, cross linked Polyethylene (XLPE) is produced to achieve higher dielectric strength and thermomechanical stability.

### 1.1.1 Polymeric materials: from insulators to conductors

Typical requirements for an electrical insulator are: it must have a high enough dielectric strength to withstand an electrical field between the conductors; it must have a high electrical resistivity to prevent leakage of current across the conductors. It must possess a good resistance to discharges to prevent damage in case of arcing. Insulating materials must be mechanically strong to resist shocks,

vibrations, and other mechanical forces. It must maintain integrity under a wide variety of environmental hazards (e.g., humidity, temperature, and radiation) [3].

To describe electrical properties of polymers means to thoroughly examine their responses to the electric field applied to them. Unlike metals, which respond readily to an electric field by electronic conduction, the response of polymers is more complex.

In general, the electric conduction in polymers is very low, which makes them useful as very effective electric insulators. If there is any conduction in a polymeric substance, it is often caused by impurities that provide tiny charge carriers in the form of electrons and/or ions. They provide very good insulation solutions but are subjected to deterioration in service under the influence of electrical, thermal stress and other degradative stresses. In addition, at sufficiently high fields, when the applied voltage exceeds a certain value, a variety of processes will cause a complete breakdown of the polymeric material serving as insulation. Their use in practical applications is for that reason limited.

The electric breakdown must be prevented, because it leads to failure of an electric component or may endanger people handling the component. Some materials are designed to work as safe insulators under low or moderate voltages, while some are developed to be used under high or extra-high voltages (HV or EHV).

High-voltage direct current (HVDC) applications are nowadays increasing and polyethylene-based materials are thermoplastic materials widely applied for HVDC cables insulation.

On the other hand there still exist some conductive or semi-conductive polymers which have a narrow band gap.

Conductive polymers, more precisely, intrinsically conducting polymers, such as polyacetylene (its high electrical conductivity was discovered in the 1970s [4] and recognized by the Nobel Prize in Chemistry in 2000) and phenylene vinylene (PPV, a famous family of semiconducting polymers and extensively used in organic light emitting diodes), are organic polymers that conduct electricity. They can have metallic conductivity or can be semiconductors. Most of the conductive polymers are not pure polymers but compounds, while even polymers themselves are not pure at all because of their degrees of polymerization and catalyst residues and impurities introduced during the manufacturing process. Their electrical and

photo-physical properties can be fine-tuned using the methods of organic synthesis and advanced dispersion techniques. Conductive polymers or conjugated polymers have drawn attention of scientists and encouraged the rapid growth of this field. Since the late 1980s, organic light emitting diodes (OLEDs) and organic photovoltaic cells have emerged as important applications of semiconducting polymers [5]. Consequently, the electroluminescence features in materials for OLEDs has been investigated extensively and deeply [6].

In general, in OLEDs there are still two basic problems or challenges: the “luminescent efficiency” and “stability” of materials and devices. The “luminescent efficiency” can be improved by specially designed structure such as electron or hole injection layers and transport layers, or by special materials such as using phosphorescent materials to replace fluorescent materials with higher luminescent efficiency. The “stability” or in another words “electrical ageing” is also a basic issue for insulating polymers in electrical applications. The ageing mechanism of semiconducting polymers and insulating polymers can be merited from each other.

## **1.1.2 A Brief History of Development in Electrical Insulation**

### **a) From oil impregnated paper to Polyethylene**

The development of electrical insulating polymeric materials is closely associated with the development of electrical apparatus [7]. In this paragraph I will briefly present an historical overview about the materials used as electrical insulator all the way up to the modern insulating polymers.

After Edison (and General Electric) lost the fight with Westinghouse and AC triumphed over DC in the early 1900's as the most appropriate form to transport electricity, it was necessary to develop electrical insulation for much higher voltages. Carefully dried paper impregnated with mineral oil was used for transformers in steel tanks and capacitors in cans at increasingly higher voltages. By 1925 oil impregnated paper, sheathed with lead, was used generally for underground cable at 13.8 kV and even up to 69 kV [8].

Many of the natural materials were extensively modified to improve their insulating characteristics. Special papers for transformers and capacitors were developed along with mineral oils selected for each application. So even before the introduction of synthetic materials a fairly wide variety of specialized, relatively inexpensive, insulating materials had been developed.

In about 1925 alkyd (saturated polyester) resins followed the somewhat earlier introduction of phenolic resins (Bakelite), as the first synthetic insulating materials. Improved heat and oil resistance won acceptance for these materials in insulating varnishes.

In 1930s poly(vinyl chloride) (PVC) was introduced to replace natural rubber in underground cable and house wiring. Resistance to fire, solvents and oil were advantageous but a low softening temperature, poor resistance to heat aging (oxidation and loss of plasticizer) and high electrical loss compared to rubber limited its application.

In about 1963 extruded polyethylene (PE) began to replace a great deal of lead jacketed, oil impregnated paper for 13 and 23 kV underground, residential distribution (URD) cable.

Failures in buried PE cable started to occur after about five years in service and were found to accelerate as time passed. At first the cause of the failures was a mystery. Voltage "treeing" was a recognized mechanism for voltage failure, but examination found an unrelated and previously unrecognized failure mechanism - "water" treeing. Over 1000 papers have now been published on water treeing and the phenomena involved still are only partly understood.

Cross-linked polyethylene (XLPE) was introduced about two years after the first use of high density PE, this is the early days of modern synthetic polymeric insulation.

From 1980s to 1990s, appeared some new concepts in high-field phenomena, such as band theory for describing the electronic properties of partially crystalline materials and field-limiting space charge for describing conduction in polyolefins. It was also the dawn of space charge measurement, i.e., the direct measurement of internal charge density distribution in bulk insulation. Several techniques such as laser-induced pressure pulse method and pulsed electroacoustic method were introduced.

From 1990s to 2000s, polymeric insulation dedicated to HVDC applications appeared as new need. The insulating materials for HVDC cables, such as XLPE, were investigated deeply.

From 2000s to present, came the nano age [7]. The booming of study on nanocomposite materials clearly marks the decade. In addition, lessons learned from space charge measurements, e.g. the bipolar nature of transport and significant injection of electronic carriers, and from electroluminescence measurements, e.g. charge recombination, have been used in an attempt to provide a complete description of insulating polymers.

## **b) Composites and nanocomposites**

Engineering plastics can be created from a single polymer, or by adding a second phase, e.g. an inorganic mineral, to form a composite. In this way it is possible to enhance key properties to render the base polymer more suitable for use in a particular application. For example Haque et. al. [9] investigated mechanical and thermal properties of glass/epoxy nanocomposites with added nanoclays such as MMT. They found significant improvements in mechanical properties with addition of 1% organo silicate nanoparticles.

While polymer composites have a long history, a critical advance in the subject occurred in the early 1990s when research at Toyota showed the benefits that can result from reducing the size of the included mineral phase. This work led to the concept of a nanocomposite, interest in which has increased at a rapid rate ever since.

In the last two decades, the design of composite materials comprising either micro-scaled or nano-scaled inorganic particles has gained increased attention in power and high-voltage engineering. Particularly, the use of micro- and nanotechnologies offers new approaches towards improved insulation systems that operate at higher temperatures and electrical stress.

Composite materials typically consist of two or more components that comprise significantly different physical and/or chemical properties. Due to the controlled combination of the components, new materials are obtained with distinct properties from the individual components [10]. If at least one of the components has nanometric dimensions, these materials are termed nanocomposites.

In the power industry, inorganic fillers particularly aluminum nitride (AlN), boron nitride (BN), silicon dioxide or silica (SiO<sub>2</sub>), aluminum oxide or alumina (Al<sub>2</sub>O<sub>3</sub>), titanium oxide or titania (TiO<sub>2</sub>), silicon carbide (SiC) and zinc oxide (ZnO), etc. are usually incorporated into electrical insulating polymers to achieve specific electrical, mechanical, and thermal properties [11].

## **1.2 Reliability of insulating materials**

### **1.2.1 Key properties of insulating materials**

With the materials improvement, intrinsic limits are being approached for understanding high field effect in insulators.

The resistance of nanocomposites to partial discharges and electric treeing enables the design of new insulation systems with enhanced electrical breakdown strength. Besides electrical properties, mechanical strength as well as thermal conductivity plays an important role in selected applications such as insulation systems of large electrical machines. In addition, permittivity and dissipation factor are desired to be as low as possible for electrical insulation whilst for capacitors, loss factor should be as high as possible. Flame retardancy is a property desired for cables insulation used in the radiation field in tunnels, while tracking resistance is very important for outdoor insulators [12].

Withstanding electrical stresses remains one of the greatest concerns for materials in electrical engineering and researches address different items, link to materials and process quality, physical understanding of processes, and design of new materials.

The greatest sources of failures are related to the presence of impurities, protrusions and voids within the polymer resulting in locally enhanced electrical stresses, which can lead to initiation of partial discharges (PD) or growth of electrical trees within the insulation [1]. All these things are known and progress in the reliability of systems has been reached by quality improvement. As now we supposedly come closer to intrinsic limit of materials, the focus in research is more on the understanding of ageing processes.

The role played by electrostatic charges, through electrostatic and electrodynamic effects is currently under the focus. Electrical charges modify the internal field distribution, leading to a critical enhancement upon voltage polarity reversal (cf. DC case below). It is also at the origin of a local material degradation upon charge recombination or hot carries effects. Through cumulative effects, it can generate large defects initiating PDs and leading to the ageing scheme explained above. Whichever the mechanism by which this ageing process occurs, it is of particular interest to understand the earlier causes of changes for the purpose of improving lifetime prediction and condition monitoring techniques.

Composites participate to strengthening materials against electrical stresses. Inorganic particles notably harden materials against the action of surface discharges. Among properties enhancement, one of the most promising with composites is the change in electric strength that has been reported when the filler particles attain nanometric dimensions.

### **1.2.2 Space charge as a threat in insulating polymers**

Electrical charging of insulating polymers, used as bulk insulation in high voltage equipment, represents a major drawback and must be avoided especially in high voltage direct current (HVDC) applications. Space charge in polyethylene-based materials still constitutes a problem affecting reliability of HVDC lines. Understanding space charge in insulating polymers has been the subject of a strong activity in the international community within the last 30 years.

Charging in these materials can occur by internal generation or by charge injection at the electrode/polymer contact. Internal generation can be linked to numerous reactions occurring under thermal/electrical stress owing to complex chemical formulation of the material with additives, such as anti-oxidants, residues, and impurities.

The accumulation of electrical charges forming internal space charge under HVDC conditions has two major consequences: (i) the internal electric field distribution is not anymore the design field. It represents a risk of formation of local domains where the higher fields values can initiate current runaway of thermal or electrical origins eventually leading to electrical breakdown [13, 14], and (ii) by cumulated

local damages to the structure of the dielectric at a molecular level. Local defects can be extended up to the stage where electrical discharges and electrical treeing can appear leading ultimately to breakdown. [15,16,17].

All these events induce a loss of system reliability. Being part of larger power systems, a local breakdown in one of the system constituents can give rise to much larger consequences (blackout of a large grid for example).

Preventing the formation of space charge in insulation is therefore a necessary step to enhance system reliability, allowing a higher level of integration of power system with the associated gain in terms of environment and space saving.

The main route followed for avoiding space charges in insulations is that consisting in improving crosslinked polyethylene regarding the amount of residues: crosslinking is known to produce polar by-products that detrimental to the DC performances by producing copious charge generation. Another way we have followed is that consisting in limiting electronic carriers generations.

Recently, a very efficient method to block charge injection was developed by inserting a nanocomposite layer between the semi-conducting electrode and the polymer: the idea consists of deposition of a semi-insulating nanoscale layer with metallic inclusions. The layer is composed of a single plane of silver nanoparticles (AgNPs) embedded in a semi-insulating organosilicon matrix deposited on the polyethylene surface by a plasma process. Control over size, density and surface coverage of the nanoparticles is achieved through the plasma process operating parameters. A drastic effect was observed and attributed to the presence of AgNPs acting as artificial deep traps for injected charges which prevent from charge injection in the polymer [18,19, 20].

### **1.2.3 Ageing Diagnosis**

Measurements of electrical properties useful for insulation characterization and for aging diagnosis were carried out by different research groups in the framework of the European project “ARTEMIS” (Aging and Reliability Testing and Monitoring of Power Cables: Diagnosis for Insulation Systems), with the aim to investigate the degradation mechanisms and to evaluate reliability of high voltage cross-linked polyethylene (XLPE) cables. Among these properties, space charge,

charging/discharging current, polarization loss and electroluminescence (EL) measurements are associated with the mechanism of charge injection and transport [21].

There is a general agreement among researchers that electrical aging of synthetic insulation used in high voltage cables could be started by space charge accumulation.

Electroluminescence emission enables a link to be made between space charge phenomenology and the release of energy due, for example, to radiative charge recombination. It is therefore of importance to be able to define levels of fields and associated space charge profiles that are liable to give rise to luminescence excitation since EL is the evidence of the existence of highly reactive excited states in the insulation that could promote accelerated aging [22].

In the next section we will introduce the phenomenon of luminescence, with particular attention to the electroluminescence in insulating polymers. Specifically we will analyse how the measurement of this feature can reveal some important detail of the materials.

## **1.3 Luminescence processes in insulating polymers**

### **1.3.1 Introduction**

Luminescence is an old technique. It's fully described for the first time by Sir G.G. Stokes who reported the theoretical basis for the mechanism of absorption (excitation) and emission. Today luminescence, in its varied forms, is one of the fastest growing and most useful analytical techniques in science. Applications can be found in areas as diverse as materials science, environmental science, microelectronics, physics, chemistry, biology, biochemistry, medicine, toxicology, pharmaceuticals, and clinical chemistry. This rapid growth has occurred only in the past couple of decades and has been principally driven by unique needs of the life sciences.

Luminescence techniques are nowadays more and more utilized because of their important advantages:

- **High sensitivity**, for highly luminescent compounds, concentrations as low as the one part per billion to one part per trillion can be detected. This is a sensitivity approximately 10,000 times greater than absorption spectroscopy.
- **Good selectivity**, specificity in luminescence arises from two factors, only about 10% of all substances that absorb radiation re-emit it as light and there are two selectable wavelengths (excitation and emission) in luminescence as opposed to only one in absorbance. It is highly unlikely that two substances will share both a similar excitation and emission. This is because the difference between excitation and emission peaks can range anywhere from several nanometers to hundreds of nanometers (UV to infrared).
- **Environmental qualitative information**, Because of the longer lifetimes involved in the electronic transitions of luminescence, it is far more sensitive to the local environment than absorbance.

In accordance with various excitation sources, there are several methods allowing the production of luminescence from dielectrics:

1. **Photoluminescence** (PL), including Fluorescence and Phosphorescence (also called UV induced luminescence);
2. **Electroluminescence** (EL), Mixture of excitation processes induced by electric field;
3. **Cathodoluminescence** (CL), induced by an electron beam;
4. Charge **Recombination** induced **Luminescence** (RL), recombination between trapped carriers, no kinetic energy;
5. **Chemiluminescence** (CHL), derives its energy from chemical reactions. It is the breaking of chemical bonds that supplies the energy;
6. **Triboluminescence**, is derived from the Greek word tribo meaning to rub. It is emitted when certain materials are stressed, crushed, or broken;
7. **Thermoluminescence** as luminescence following sensitization through e.g. ionizing radiation followed by heating inducing charge detrapping and recombination

### 1.3.2 Photoluminescence – optical excitation

Photoluminescence is light emission from materials after the absorption of photons (electromagnetic radiation). Photoluminescence is further divided into categories: fluorescence and phosphorescence. Today they are defined via the emission based on quantum mechanical mechanism for the orbital angular momentum multiplicity of the emitted electron (i.e. the singlet or triplet excited states). However, before the advent of quantum theory photoluminescence was defined on the basis of empirical evaluation of the duration of emission lifetime. The process can be described as: the material absorbs photons, to be excited to states at high energy level, then release back to the ground state, meanwhile emitting light. The emitted light has a lower energy and therefore longer wavelength than the excitation light.

#### a) Fluorescence

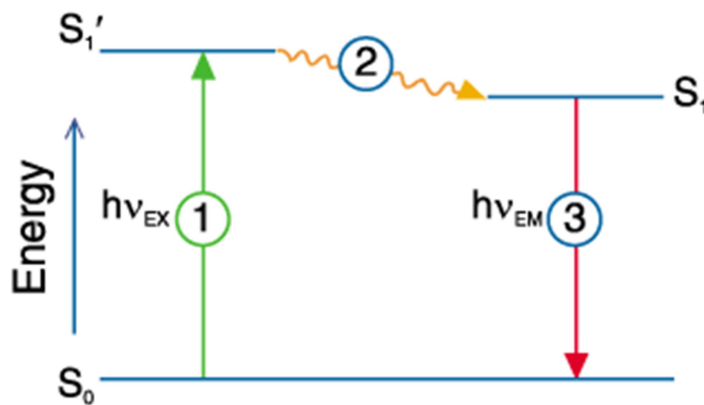


Figure 1 - 1: representation of Fluorescence stages.

#### Stage 1: Excitation

A photon of energy  $h\nu_{EX}$  is supplied by an external source such as an incandescent lamp or a laser and absorbed by the fluorophore, creating an excited electronic singlet state ( $S_1'$ ), cf. Fig. 1-1.

#### Stage 2: Excited-State Lifetime

The excited state exists for a finite time (typically 1-10 nanoseconds). During this time, the fluorophore undergoes conformational changes and is also subject to a multitude of possible interactions with its molecular environment. These processes have two important consequences. First, the energy of S1' is partially dissipated, yielding a relaxed singlet excited state (S1) from which fluorescence emission originates. Second, not all the molecules initially excited by absorption (Stage 1) return to the ground state (S0) by fluorescence emission. Other processes such as collisional quenching, fluorescence resonance, energy transfer and intersystem crossing may also depopulate S1. The fluorescence quantum yield, which is the ratio of the number of fluorescence photons emitted (Stage 3) to the number of photons absorbed (Stage 1), is a measure of the relative extent to which these processes occur.

### **Stage 3: Fluorescence Emission**

A photon of energy  $h\nu_{EM}$  is emitted, returning the fluorophore to its ground state S0. Due to energy dissipation during the excited-state lifetime, the energy of this photon is lower, and therefore of longer wavelength, than the excitation photon  $h\nu_{EX}$ . The difference in energy or wavelength represented by  $(h\nu_{EX} - h\nu_{EM})$  is called the Stokes shift. The Stokes shift is fundamental to the sensitivity of fluorescence techniques because it allows photons emission to be detected against a low background, isolated from excitation photons. In contrast, absorption spectrophotometry requires measurement of transmitted light relative to high incident light levels at the same wavelength.

### **b) Phosphorescence**

Phosphorescence occurs when the material does not emit light immediately after being excited, due to the energy transition in quantum mechanics.

As we can see in the figure 1-2, we have a first stage in which the material is excited to higher energy states, then undergo an intersystem crossing into energy state of higher spin multiplicity, the singlet change his status and a part of the energy is used to do a spin-flip, from a singlet to a triplet S1→T1 (intersystem

crossing). Normally the transition  $T1 \rightarrow S0$  is forbidden, which is why the lifetime of triplet states (phosphorescence) is longer than that of singlet states (fluorescence).

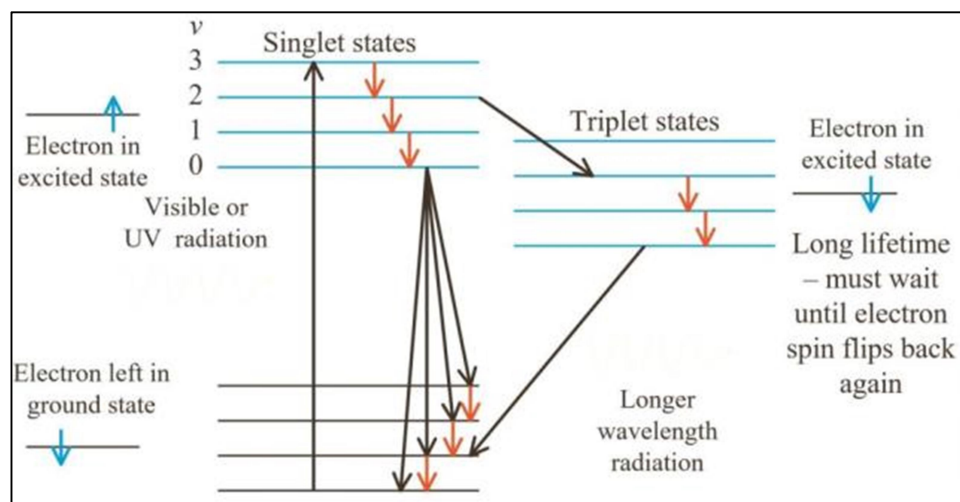


Figure 1 - 2: Phosphorescence main stages.

### 1.3.3 Electroluminescence

Electroluminescence is the light emitted by a solid through which an electric current is passing, in addition to its normal thermal emission. It implies the presence of electronic excited states with populations larger than their thermal equilibrium value.

Most of the electroluminescent solids are semiconductors. Light is produced by recombination of electrons and holes that have been injected at the cathode and anode respectively.

Electroluminescence was first observed in silicon carbide (SiC) by Captain Henry Joseph Round in 1907. Round reported that a yellow light was produced when a current was passed through a SiC detector. The second reported observation of electroluminescence did not occur until 1923, when O.V. Lossev of the Nijni-Novgorod Radio Laboratory in Russia again reported electroluminescence in SiC crystals.

Electroluminescence in organic semiconductors was firstly reported in 1963 and exploited as organic light emitting devices. On the other hand, electroluminescence in insulating polymers was firstly reported in 1967. So far, EL

in Polyethylene (PE), Polypropylene (PP), Polyethylene terephthalate (PET), Polyethylene Naphthalte (PEN), Polytherimide (PEI), Polyimide (PI), Polyethersylfone (PES), Polyvinyl Chloride (PVC), et. al., have been observed and studied.

In EL, electrical energy is transformed into light. To radiate in the visible portion of the spectrum, the luminescence centre must have an excited state of  $\geq 2$  eV higher than the ground state. The most important and interesting issues to reveal are: as how the radiative system is excited, and as which the light generation mechanism itself is.

### a) Electroluminescence mechanism in dielectric materials

In electroluminescence we have electric field as excitation source, it follow different excitation processes. In the Figure 1-3 is shown the energy band diagram of conductor, semiconductor and insulator (dielectric).

The most straightforward mechanism of EL excitation is direct field ionization of a centre. This effect involves electron tunnelling from the valence band to the conduction band (Zener effect) which occurs in semiconductors with a band gap of about 1-3 eV. It could not play any role in a large band gap insulator (beyond 5 eV).

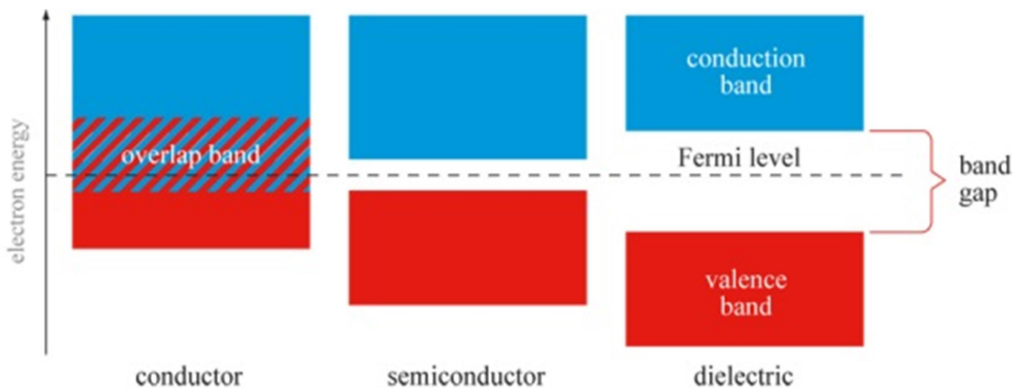


**Figure 1 - 3:** band gap in conductor, semi-conductor and dielectric materials.

A second excitation process is the inelastic collision of a high energy electron, a so-called hot electron, with a centre (Destriau effect). The kinetic energy of the carriers is directly involved in the excitation process. A third mechanism is bipolar

charge carrier generation and subsequent electron-hole recombination which does not involve carrier kinetic energies, but does involve their potential energies. These last two processes have been studied quite extensively in connection with the dielectric breakdown strength of solids.

The excitation process in insulating polymers is localized in given molecular orbit or at luminescent centres, leading to the formation of excitons. An exciton is a bound state of an electron and a hole that are attracted to each other by the electrostatic Coulomb force, which is regarded as an elementary excitation that can transport energy.

### **b) Relaxation process and possible luminescent centres**

Once the excited state has been formed, its de-excitation involves different pathways. Among the different possible mechanisms, one can distinguish two main classes: chemical, i.e. irreversible pathway and physical, i.e. reversible pathway. Both this classes of transitions can be radiative and non-radiative. In a physical process, the excited centre returns to its ground state without any chemical reaction. In a chemical reaction, the excited states can dissociate into molecular fragments which can be very reactive and lead to further chemical reactions. The balance between these two mechanisms is obviously very important for the relationship between electrical degradation and EL emission. If EL involves only physical processes, it would be a way to probe the excitation rate. If chemical processes are involved, EL can also be due to radiative de-excitation of degradation products and could provide a way to measure the dissociation rate. So in both cases, EL is considered as a potential ageing warning.

In relation to the luminescent centres, the pure carbon chain C-C or C-H single bonds in insulating polymers cannot perform as luminescent centres in the UV-visible domain, because the energy level transitions in these bonds are transitions at the extreme ultraviolet domain with high energy (8 eV or so).

Therefore, in a polyolefin polymer like polyethylene or polypropylene, there is normally no emission from the repeat unit due to aliphatic structure of the chains. So, if luminescence is detected, it is necessarily due to some types of possible chromophore groups in the carbon chain.

However, which chemical structure is actually excited and act as the chromophore under electrical field is still unknown issue according to previous works. It is still difficult to localize the definite luminescent centres by experimental work and simulations. Nevertheless, spectral analyses can help to investigate the source of the light emission. Works are carried out to uncover the nature of luminescent centres in these insulating polymers.

A further difficulty is the possible involvement of electrode related emission –so called surface plasmons –SP- as explained below- when using gold or silver as electrodes for the material: the emission from insulating material would be superimposed to that from the electrodes. Figure 1-4 shows an example of such spectra obtained on XLPE with Ag electrodes [23] where emission at 750 nm has been ascribed to SP emission.

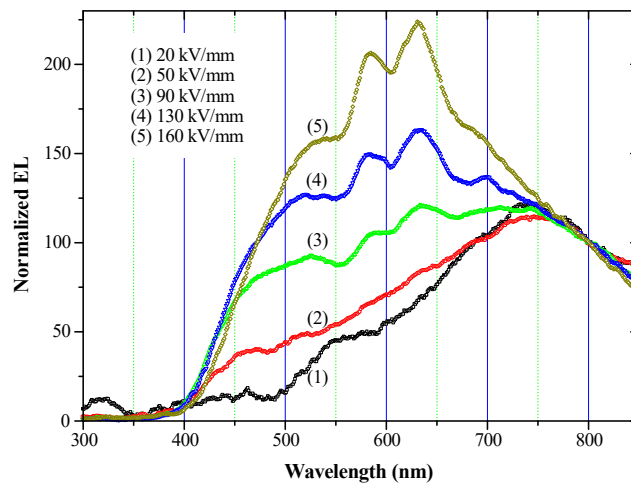


Figure 1 - 4: AC-EL spectra from Poly(ethylene naphthalate) films with Ag electrodes [23].

### c) Electroluminescence and electrical ageing

The dielectric materials could be subjected not only to electrical stress but also to thermal, mechanical, chemical and environmental stresses. The mutual action of these stresses causes chemical changes to the polymer, eventually resulting in degradation and catastrophic failure of the system.

The mechanisms of ageing in insulating polymers submitted to electrical stress are not well known from a chemical standpoint, partly because of lack of techniques that are sensitive enough to detect the mild changes which are produced, and

partly because a low level of degradation is sufficient to initiate breakdown. Electric fields, through space charge effects, may produce excited or ionized states of the constitutive groups of the polymer, which can be involved in a subsequent chemical reaction. Some of these excited species have a non-zero probability for light emission during their relaxation. This light is called electroluminescence (EL). Therefore, the EL should in principle bring information on the nature of the recombining centres, which may have some relation with the initial centres of degradation. For the above described reasons the EL is an appropriate technique to detect the initiation of electrical breakdown in insulating polymers. Hence, EL is of double interest: on the one hand, it may provide information on the stress threshold for degradation and, on the other hand, it may help in identifying the nature of the defects where degradation originates.

The ageing sources can be several. They may have different origins: electrical, mechanical, ultraviolet (UV), chemical, thermal and water stresses. Each source may cause different ageing mechanism and thus to affect the electrical insulation in different ways. They could all have an influence on the formation of space charge (SC) within the polymer.

Furthermore, the EL is the only direct experimental evidence of the existence of potentially dangerous excitation energy in insulating polymer during ageing.

An important characteristic of EL, detected in many different polymers under AC and DC fields is that the light emission increases linearly with the applied field above a critical value.

The onset of EL changes from an insulating polymer to another due to their intrinsic electrical properties, for that reason we can say that onset of EL corresponds to the start of excitation mechanism which is universal among the insulating polymers. The EL onset voltage could represent a warning of electrical ageing.

With luminescence techniques, we can carry out light emission from each single process, such as recombination process and chemical reaction process, for analysing. This provides more information of EL, which proves EL is a multi-excitation involving physical and chemical processes under electric stress.

## 1.4 Surface Plasmons

We have briefly addressed above the possibility that EL from Ag or Au metallized samples be partly due to emission radiated during relaxation of surface plasmons. We describe here the nature of surface plasmons.

### 1.4.1 Introduction

A plasmon is a quantum of plasma oscillations. Just as light, viewed as optical oscillation, consists of photons, the plasma oscillation consists of plasmons. The plasmon can be considered as a quasiparticle since it arises from the quantization of plasma oscillations, just like phonons are quantization of mechanical vibrations. Thus, plasmons are collective (a discrete number) oscillations of the free electron gas density. For example, at optical frequencies, plasmons can couple with a photon to create another quasiparticle called a plasmon polariton [24].

Volume plasmons in a metal are longitudinal density fluctuations of the electron gas, plasma oscillations that propagate through the metal. They can be excited by a supply of energy, through either photon or electron irradiation. The quanta of these volume plasmons have energy  $\hbar\omega_p = \hbar\sqrt{4\pi ne^2/m_0}$ , (of the order of 10 eV), where  $n$  is the conduction electron density,  $\hbar$  is the reduced Planck constant,  $\omega_p$  is the plasmon frequency,  $e$  is the elementary charge and  $m_0$  is the electron mass. They are produced by electrons which are shot into the metal.

An important extension of the plasmons physics has been accomplished by the concept of surface plasmons (SP). By extension a SP can propagate along a metallic-dielectric interface with a broad spectrum of eigen-frequencies from  $\omega_{SP} = 0$  to  $\omega_{SP} = \omega_p/\sqrt{1+\epsilon_d}$ , depending on the wave vector  $k$ . The frequency of a SP in a metal is thus necessarily lower than that of volume plasmons. The electromagnetic field has a maximum at the metal-dielectric interface and decays exponentially in the direction perpendicular to the interface, as is characteristic for surface waves, cf. Figure 1-5.

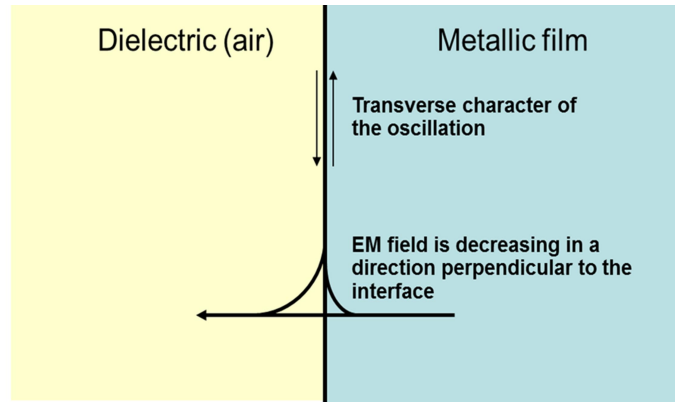


**Figure 1 - 5:** interaction between a metallic and a dielectric medium.

## 1.4.2 Coupling surface plasmons and photons: conditions for radiative relaxation

SPs at a perfectly smooth interface do not radiate light because their momentum  $k_{SP}$  is parallel to the surface and it is always greater than the momentum  $k_{ph}$  of photons of the same energy. The coupling conditions between the two particles are the energy conservation and the momentum conservation. If we can consider the same energy for SP and photon, the same cannot be said about the momentum.

This prevents the momentum conservation condition to be fulfilled which states that during the coupling, the components of the momentum of the two quanta parallel to the surface,  $k_{\parallel}$  must be conserved.

The surface roughness, as we can see in figure 1-6, provides smaller components of the SP wave vector parallel to the surface  $k_{\parallel}$ , leading to the possibility of radiative decay of SP in the visible domain.

The scale of roughness which is needed to couple SP with optical photons is from 1 to 100 nm, features that are naturally obtained with metallic layers deposited by conventional methods, sputtering of a metallic target or thermal evaporation of a metal.

The radiative de-excitation of SP has been observed in various metal-insulator-metal (MIM) structures biased under different voltages. In tunnelling junctions, a

thin insulating layer ( $\approx 10$  nm) is used to control the tunnelling current which excites SP on the electrodes. The effect is similar to that obtained in a scanning tunnelling microscope.

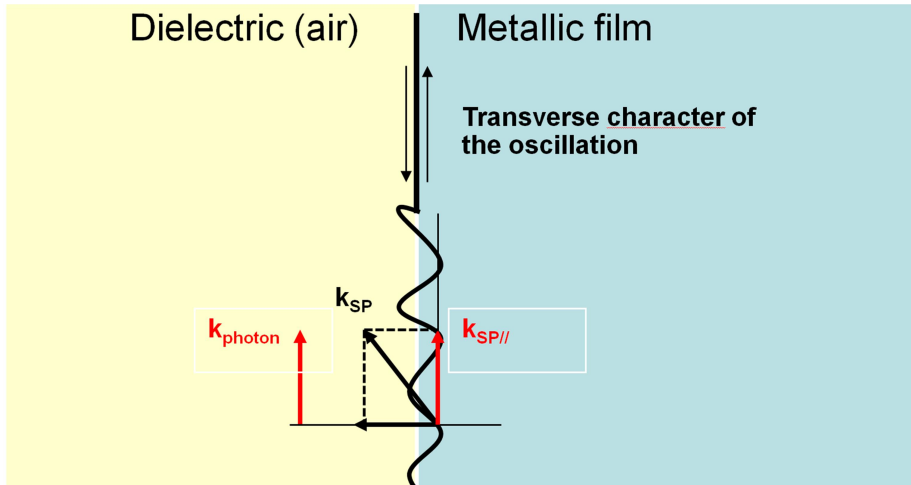


**Figure 1 - 6:** Interaction between a metallic film and a dielectric medium in presence of a rough surface. Coupling condition for a surface plasmon and a photon.

### 1.4.3 Spectral distribution of the light emitted by SP

The other necessity is having a volume plasmons in the relevant energy range (visible or UV), as in the case for noble materials (Ag or Au). The maximum frequency of the optical emission  $\nu_{max}$  follows the relation  $eV_0 = \hbar\nu_{max}$ ,  $e$  being the electronic charge and  $V_0$  the voltage applied between the electrodes of the MIM structure or between the electrode tip and the metallic surface in the tunnelling microscope [24].

Consequently, the spectral distribution of the light emitted by SPs depends on the properties of the metallic layers and the excitation conditions. The shape of the spectral output depends on several factors, such as: the energy distribution of the carriers that excite the SP modes, the surface roughness profile of the electrode, the energy-dependent internal damping of SP modes. It follows that there is variability in the emission spectrum due to SP from one sample to the other. On the other hand, the optical emission due to SP excited on different metallic layers,

especially in gold electrodes, exhibits an emission spectrum peaked in the red (620 to 850 nm) over a wide range of excitation conditions.

#### 1.4.4 SP implication in electroluminescence spectra

The implication of SP in the red component of EL is consistent with several experimental observations. For example, in the Figure 1-7 we can see the emission spectra of an AC field EL for different MIM structures.

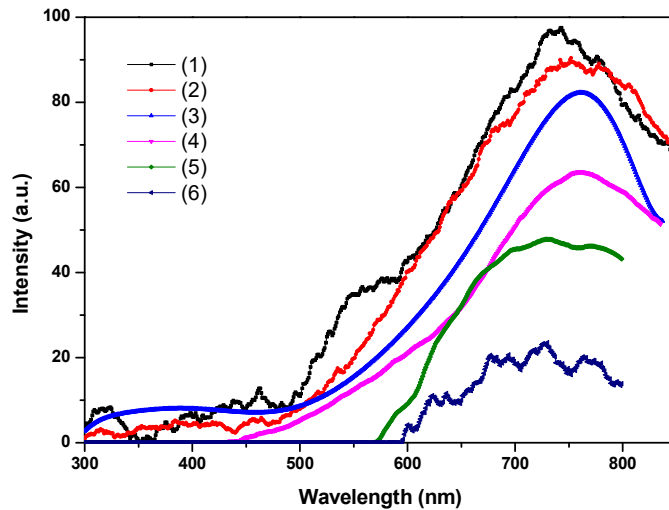


**Figure 1 - 7:** Emission spectra due to SPs related emission in Metal-Insulator-Metal structure of different nature. Low field EL spectra of (1) Ag-Polyethylene Naphthalate-Ag, (2) Ag-PE-Ag and (3) Au-PE-Au, (4) due to surface plasmon in a MIM structure. (5) SPs from BOPP, (6) SPs from XLPE.

The excitation of SP by charge injection/extraction needs a critical current density at the electrode surface. Imaging EL in the plane of the sample gives the relevant information to discuss this process in the case of highly resistive materials such as PE and PEN.

Under DC excitation, for example, the emission spectrum does not exhibit any particular emission in the red, i.e. the conditions for SP excitation are not fulfilled.

To the contrary, imaging shows a strong localization of the emission at preferential spots in the sample plane when EL is excited under AC conditions, and the emission spectrum exhibits the red component. In the latter case, conditions are fulfilled for SP excitation.

Under AC stress, alternative injection and extraction of charge carriers at the electrode surface leads to high local current density around the sites which favour charge transfer, and thus SP excitation by charge injection/extraction can be fulfilled. Under DC, injection starts around the same sites, but due to the screening effect of the charge, the field is relaxed around these spots. EL is excited in the bulk material and SP excitation is not fulfilled at the electrodes [24].

There are many experimental facts inclining, as we said, for an emission process occurring at the contact of electrode/polymer under AC, due to charge injection-extraction at the interface. This also explain the fact that the red component is not detected under DC because the EL comes from the bulk of the sample, in that case, contrary to the AC where charge exchange is mainly occurring at the contact.

Another theme we will debate in this dissertation, with the support of some experimental measurements, is the fact that the red component is not observed with ITO electrodes under AC, this is another evidence that the source is located at the contact.

### **1.4.5 Silver nanoparticles (AgNPs) as the most appropriate nanostructures to support surface plasmons**

Noble metallic nanoparticles (NPs) are widely studied for different applications like for enhanced optical spectroscopies of molecules [25], nonlinear optics [26;27], photothermal therapy [28], photovoltaics [29;30], biocide effects [31;32] or more recently in plasmo-electronics [35;34], photocatalysis [35;36;37] and charge transport control [19] but mainly for their exceptional optical properties. In the past decade, a particular attention was paid on noble metallic NPs because they support localized surface plasmon resonance (LSPR). These collective oscillations of the conduction band electrons enable strong optical absorption and scattering in subwavelength structures, with spectral properties depending on the NP material, size, shape, electronic charge and surrounding medium. Among all noble metal NPs, AgNPs realize the best nanoscale antennae in the visible range of the spectrum (Figure 1 – 8). In this section, we will briefly describe the electronic and optical properties of noble metal NPs.

Scaling down to nanometer size, the optical response of metals is affected by three main features: size, shape and surrounding medium of the metal. The complex dielectric function of metal nanoparticles develops size dependency in the nanometer range. The size dependency of dielectric function stems from both interband transitions and damping contributions with the later contribution usually exceeding. The damping involves changes in the electronic mean free path due to the scattering of conduction electrons against the nanoparticle surface.

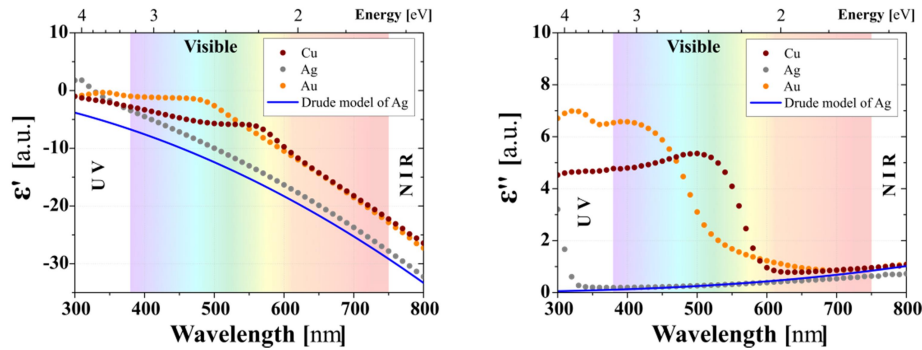


**Figure 1 -8:** Experimentally obtained real part  $\epsilon'(\lambda)$  and imaginary part  $\epsilon''(\lambda)$  of the dielectric function of Cu, Ag and Au (color points) for bulk materials. The blue line represents the calculated dielectric function according to Drude model. Adapted from A. Pugliara [38].

In the same way that we have described the surface plasmons along the metal/dielectric interface, we can define the localized surface plasmon as the quantum of collective oscillations in a NP. The corresponding resonance or LSPR takes place for a frequency:

$$\omega_{LSPR} = \frac{\omega_p}{\sqrt{\epsilon_{IB} + 2\epsilon_d}},$$

where  $\epsilon_p(\omega)$  is the plasma frequency,  $\epsilon_{IB}(\omega)$  is the part of the complex dielectric function due to the interband transitions in bulk metals and  $\epsilon_d(\omega)$  is the dielectric function of the surrounding dielectric medium. This frequency depends on the NP material and shape (here the factor 2 is the shape factor for a sphere) but also on the environment ( $\epsilon_d$ ) of the NP. Thanks to their small size, the NPs allow to concentrate the electromagnetic field at a scale drastically smaller than the corresponding wavelength. This is particularly suitable to the use of the exaltation

effects of the light diffusion by objects localized in their near field as the well-known SERS (Surface Enhanced Raman Spectroscopy) effect [39].

The resonance frequency  $\omega_{\text{LSPR}}$  of a spherical NP, and therefore the associated photon energy, depends on the nature of NP material but also on that of its embedding matrix. We can hence calculate the resonance energy of the composite system if we know the dielectric functions of the both materials. The calculation of the extinction efficiency gives information on the resonance profile (frequency location, width and intensity) and allows the best choice of the couple (NP material/matrix). In Figure 1 - 9, the extinction coefficient for NPs made of 3 noble metals (Ag, Au and Cu) in two different matrices ( $\text{SiO}_2$  and  $\text{Si}_3\text{N}_4$ ) is plotted [39]. The relative amplitude of each curve clearly shows an important resonance for Ag and Au that can be used for plasmonic applications in these two types of matrices. Nevertheless, the Ag resonance is clearly higher than the one of Au and this material is better for maximum field exaltation. Indeed, the resonance quality factor, defined as  $Q = \lambda_{\text{LSPR}}/\Delta\lambda$  where  $\Delta\lambda$  is the FWHM, is higher for AgNPs than for AuNPs (metal effect) because of the supplementary damping by interband transitions in Au. By changing the embedding medium, from  $\text{SiO}_2$  ( $\epsilon_{\text{SiO}_2} = 3.9$ ) to  $\text{Si}_3\text{N}_4$  ( $\epsilon_{\text{Si}_3\text{N}_4} = 7.5$ ) for example, a strong enhancement of the LSPR and tuning in the middle of the visible can be obtained. The LSPR of AgNPs shifts from the near UV range (400 nm) to the visible range (475 nm). Owing to the fact that the higher the refractive index, the better the electromagnetic energy confinement is, the quality factor is doubled when changing the surrounding medium from  $\text{SiO}_2$  to  $\text{Si}_3\text{N}_4$  for example. Nevertheless, most of the studies in the literature describing AgNPs embedded in dielectrics for plasmonic applications involve silica matrices. The optical response of AgNPs is used in this work for non-destructive characterization of polymeric materials.

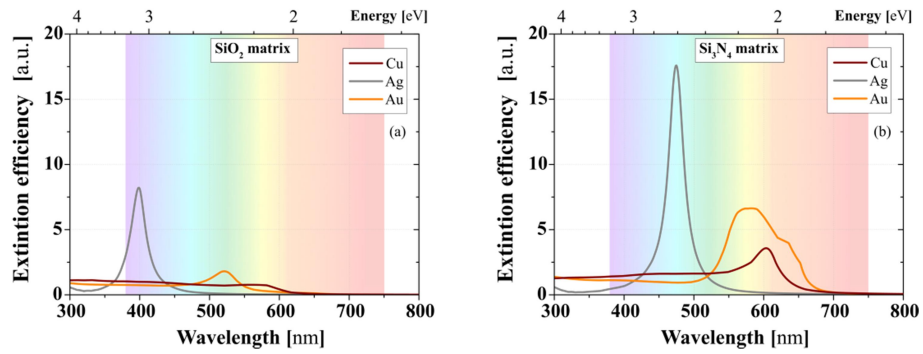


**Figure 1 - 9:** Extinction efficiency of noble metal NPs embedded in a  $\text{SiO}_2$  (a) and  $\text{Si}_3\text{N}_4$  (b) matrix [39].

## 1.5 Purpose of the thesis

The idea of this dissertation is to start from the results obtained by B. Qiao in his thesis and, during the first part of this work, to repeat some experimental measurements aiming at a firm confirmation of the observed features.

For this reason, our samples will have MIM (Metal-insulator-metal) configuration. The metal deposited on the polymers, BOPP (Bi-axially Oriented Polypropylene), will be gold (Au) or ITO (Indium Tin Oxide).

In the figure 1-10 we can see the experimental situation with gold as semi-transparent metal sputtered on the surface of the insulator.

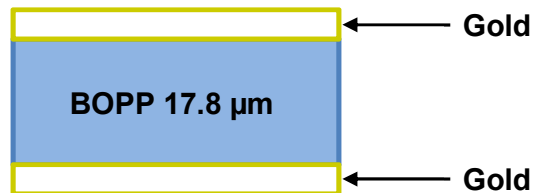


**Figure 1 - 10:** structure of an Au-BOPP-Au sample.

In this case, during EL measurement, surface plasmons are generated by electronic current due to polarity change with two possible origins (cf. Fig 1-11):

1. Injection or extraction of current at the metal(electrode)/dielectric interface;

2. Surface current between metallic particles in case the electrode not constitute a perfectly continuous layer. We remind that thin metallic electrodes are used (come tens of nm thickness) to get reasonable light transmission through it.

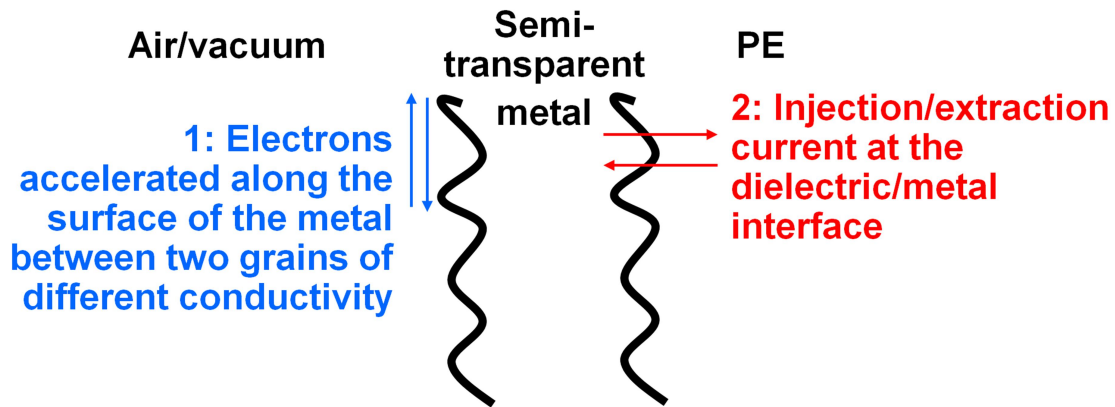


**Figure 1 – 11:** Interaction between vacuum, metal and BOPP. Two SP can potentially develop: at dielectric-Au interface and at Au-vacuum interface.

In Figure 1-12 we can see a schematic situation during the positive half cycle applied to the electrode all along an EL measurement:

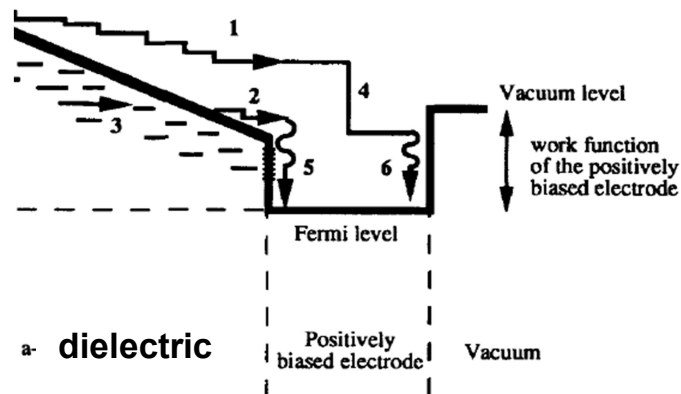


**Figure 1 – 12:** Interaction between vacuum, metal (electrode) and BOPP.

- Electrons with a low kinetic energy (2) or trapped near the interface will be collected by the metal and relaxed at the dielectric-metal interface (5).
- Electrons with a higher kinetic energy (1) can be injected into the metal and relaxed (4) on their way to the metal-vacuum interface. If they have sufficient kinetic energy, they can excite SP at the interface (6). This will depend on: the kinetic energy of the electron, the thickness of the metallic layer, the scattering length of hot electrons into the metal. Thickness of 100 nm to 500 nm is pertinent for kinetic energies of 10 eV.

In the second part of my work intends to check the SP hypothesis by changing the structure of the sample. The idea is to keep the same arrangement, same thickness of the different layers, and to deposit a mono layer of AgNPs embedded in an organosilicon (SiOC:H) matrix on the top of BOPP substrate. Although the SiOC:H matrix is known as low-k material, with dielectric constant between 2.0 and 3.0 depending on the elaboration process, it was selected to better adapt to the polymer (plastic) substrate. Then cover both sides with an ITO layer to form the final structure under study, cf. Fig. 1-13.

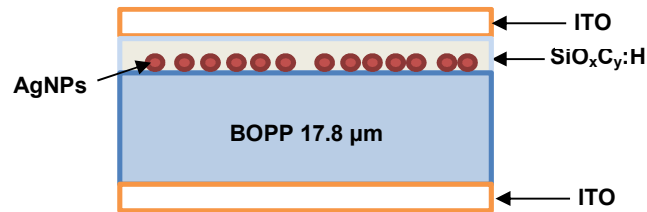


**Figure 1 - 13:** Structure of the multi-layer sample (ITO-BOPP-AgNPs- SiO<sub>x</sub>C<sub>y</sub>:H-ITO).

The investigated process will be the impact of the confinement of the metal into nanoparticles on the SPs effects, along with supporting information on the role of deep traps from AgNPs previously reported under DC stress.

## **1.6 Plasma deposition techniques for synthesis of AgNPs in silica-like matrix**

One of the purposes of this thesis will be to investigate EL from metallic nanoparticles containing nanocomposite ultra-thin films. Therefore we purpose a brief state of the art on deposition processes.

### **1.6.1 Introduction**

Plasma based deposition of thin films is largely applied in industrial applications [40]. Starting in the microelectronic domain in the early 80's of the last century, the plasma technologies for deposition have now place in different areas of our every day's life, like for example in optics for coating layers, for surface treatment in the food industry, for biomedical applications, in photovoltaics', etc. Depending on the type of the used gas discharge, the main plasma characteristics (electron density and electron energy), the reactive gases injected as precursors and the gas pressure, one can obtain a quite large variety of composition of deposited thin layers, including elaboration of nanocomposite materials. Principally, the Physical Vapor Deposition (PVD) and the Plasma Enhanced Chemical Vapor Deposition (PECVD) are used in the surface modification of a wide range of substrates. In particular, PVD involves the evaporation or sputtering of a solid material while in PECVD the plasmas are used to activate the chemical precursors and consists of applying different types of gas discharges. The advantage of these deposition methods concerns the huge versatility and the excellent control of thin film growth at micrometric and nanometric scale [18;19;31;32;40;41;42;43;44;45;46] Industrial plasma reactors are usually supplied with alternative current (AC) and depending on the used gas discharge they work in the whole range of pressure variation, from low pressure up to atmospheric pressure. Without loss of generality the discussion here is limited to an axially-asymmetric radio-frequency (RF) capacitively-coupled discharge sustained at 13.56 MHz at low gas pressure. This plasma deposition process has been chosen to elaborate a layer of AgNPs embedded in the organosilicon layer for our studies.

## 1.6.2 Plasma Enhanced Chemical Vapor Deposition (PECVD)

Versatility of plasma based deposition processes is widely used for technological purposes. Plasma enhanced chemical vapor deposition (PECVD) processes have now place in different areas of our every day's life, like for example in optics for coating films, for surface treatment in the food industry, for biomedical applications, in photovoltaics' domain, etc. [40]. Depending on the type of operated gas discharge, the main plasma parameters (electron density and electron energy), the reactive gases used as precursors and gas pressure, one can obtain a large variety of composition of the deposits, including nanocomposites [44]. The possibility to design complex nanocomposite thin layers is determined by the complexity of the medium itself. The properties of non-equilibrium plasmas as media actually represent key elements in the synthesis of nanocomposite thin films offering a high degree of freedom in their elaboration.

RF capacitive coupled discharges are by far the most widely applied ones for thin film depositions, entirely compatible with the microelectronic technology. Moreover, in hybrid plasma deposition methods, by combining PECVD and sputtering, nanoparticles can also be composed of the sputtered material [41;43]. Such systems thus represent interesting building blocks for deposition of multifunctional, nanocomposite thin films. Nanocomposite materials consisting of AgNPs embedded in dielectric matrices present a huge interest as plasmonic substrates. The main advantage of these assemblies is the possibility to manipulate, localize and enhance the electromagnetic field at the structure surface. To take benefit of the hybrid plasma deposition when the sputtered target is a silver material at LAPLACE Laboratory they have developed a strategy to elaborate large area plasmonic substrates [32; 46; 47].

In the electrical engineering domain, the phenomenon of charge injection in dielectric layers under electrical stress is at the origin of space charge formation. For many industrial purposes, like for high voltage DC (HVDC) applications (e.g. HVDC cables with polymeric insulation), the space charge must be avoided because it gives a contribution to the electric field distribution by modifying the latter compared to the

designed one and represents a risk for breakdown, especially under voltage reversal [48; 49; 50]. In order to resolve this problem, in views of the intrinsic difficulty in controlling the contact between polymeric material and the electrode (metal or semi-conductor), the solution can be to use a thin layer of nanocomposite material with adequate properties in between the electrode and the polymer to control the injection process to the polymeric material defects or traps. This nanocomposite layer contains a single layer of AgNPs embedded in an organosilicon matrix. Due to the ability of AgNPs to store electrical charges they are supposed to play the role of deep trapping centres thereby stabilizing the injection, implying thus a field reduction at the electrode when the nanograins are charged. The control of charge injection phenomenon certainly improves the performance and increases the reliability of dielectric materials [18; 19; 20; 51]. The addition of AgNPs layer on our BOPP substrate with the application of a plasma deposition process, we want to tailor the surface of the dielectric materials by a multifunctional layer for elaboration of large-plasmonic embedded substrates. After that the mission is to investigate the optical properties of the new multilayer sample to understand the effect of AgNPs.

# Chapter 2 Experimental Materials and Techniques

## 2.1 Materials (Polypropylene)

Polypropylene (PP) is a polyolefin, composed of monomers  $-C_3H_6-$ , with the chemical formula  $(C_3H_6)_n$ , widely used in industries since invented in the early 1950s. The commercial production of PP began in 1957 in USA and 1958 in Europe [56]. It is a thermoplastic polymer widely used in a variety of application including packaging, textiles, and electrical equipment components, such as capacitors and electrical accessories. It is liable to chain degradation from exposure to heat, UV radiation, and under electric field.

Samples are extruded between two rolls and manufactured in thin films for capacitor applications with high breakdown strength.

When Polypropylene film is extruded and stretched in both the machine roll direction and across machine roll direction, it is called Bi-axially Oriented Polypropylene (BOPP). All the measurements are carried out in this dissertation on BOPP films of 17.8  $\mu\text{m}$  thickness supplied by KOPAFILM, Germany. The films were provided with different roughness for the faces, to favour oil impregnation.

The only known additives contained in the BOPP films under study are pentaerythritoltetrakis (3,5-di-tert-butyl-4 hydroxyhydrocinnamate) and calcium stearate. The former is known as Irganox 1010, which is a sterically hindered phenol used as an antioxidant to abstract unstable radicals. Calcium stearate is a lubricant and an acid scavenger used to neutralize any hydrochloric acid generated from reactions between the hindered phenol and residual chloride-containing catalyst [53].

## 2.2 Experimental setups

In the dissertation, Leica EM ACE600 system is utilized to deposit gold (Au) and Indium Tin Oxide (ITO) electrodes. Figure 2-1, represents a picture of the Leica EM ACE600 system. It is a versatile high vacuum film deposition system designed to produce very thin, fine-grained and conductive metal and carbon coatings for high resolution analysis, as required, for example, for FE-SEM and TEM applications. This high vacuum coater can be configured for the following methods: Sputtering, Carbon thread evaporation, Carbon rod evaporation, E-beam Evaporation and Glow discharge.



**Figure 2 - 1:** Leica EM ACE600 system.

The luminescence analysis system used in this work is a lab-made test bench to measure the photoluminescence (including fluorescence and phosphorescence), electroluminescence, and cathodoluminescence from solid materials.

For the AgNPs deposition a special plasma reactor developed in LAPLACE is used: it exploits the plasma of an axially-asymmetric capacitively-coupled RF (13.56 MHz) discharge sustained at low gas pressure.

## 2.2.1 Sample preparation

### a) Gold metallization setup

To perform the EL measurements, electrodes must be deposited on the studied samples to apply a controlled electric field. Besides, the deposited electrodes must be partially transparent in the UV-VIS domain in order to collect light.

The films are deposited uniformly at a deposit rate of 54.6 nm/min. The insulating polymer films are thus provided with gold electrodes having diameter of 50 mm and a thickness of 30 nm. The parameters of the sputtering are listed in Table 2-1. The sputtering pressure is about 1.5 Pa in Argon plasma. The current is 125 mA.

Sputtering	Value
Rate	54.6 nm/min
Gas	Argon
Pressure	1.5 Pa
Time	33 s
Current	125 mA
Thickness	30 nm

Table 2 - 1: Parameters of the sputtering process of gold.

### b) ITO sputtering setup

The Leica EM ACE600 system can also be used to deposit Indium Tin Oxide (ITO) on the surface of a polymer films. Improvement of this industrial system has been made by the technical staff of LAPLACE, especially to improve the vacuum level and purity of the Argon into the deposition chamber. The deposition rate, in this case, is different: 11.7 nm/min. Also the deposition time change with this process:

11.53 min. The transparency of ITO is approximately 90 %, while the surface electrical resistance is found  $16 \times 10^{-3} \Omega/\text{cm}^2$ .

Sputtering	Value
Rate	11.7 nm/min
Gas	Argon
Pressure	1.5 Pa
Time	11.53 min
Current	125 mA
Thickness	135 nm

**Table 2 - 2:** parameters of the sputtering process of ITO.

### **c) Treatment of electrode edges**

At the end of the sputtering process (Gold or ITO), before introducing the sample inside the multi-purpose chamber, it is necessary to apply a layer of silicone elastomer along the border of the sputtered zone. The ribbon avoids discharges and flashovers due to field strengthening at electrodes edges. To do so, a protective film (PP) is pressed on the silicone and kept in place for one or two days up to complete the vulcanisation in air. During my stay at LAPLACE laboratory I've developed a new process to apply the silicone elastomer and the protective film to reduce the process time and to improve removing the protective film without damaging the sample.

The new process involves making a hole (diameter of 44 mm) with a hollow punch in the protective PP film and applying the holed film on the silicone. It is possible in this way to run the EL measurement without removing the protective film. In the Figure 2-2 we can see a picture of the complete sample with Au electrode.

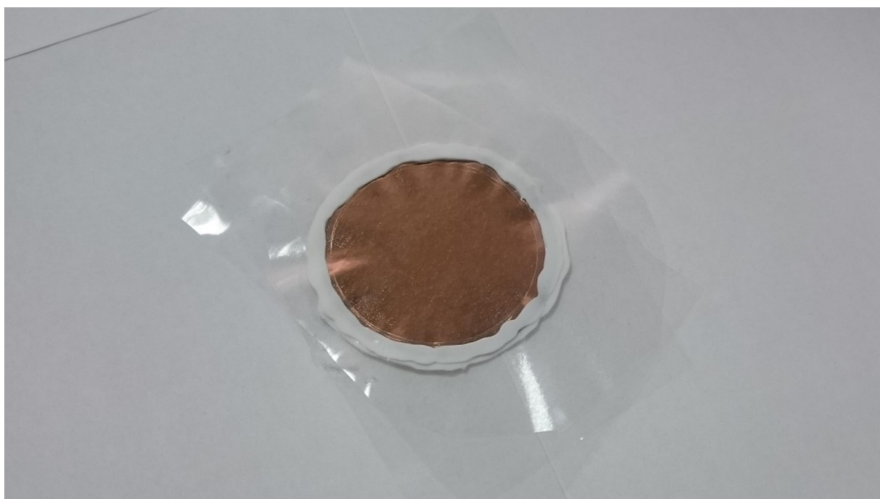


**Figure 2 - 2:** picture of a complete Au-BOPP-Au sample.

## 2.2.2 Luminescence setup

All the luminescence experiments were carried out in a multi-purpose chamber as shown in Figure 2-3. It mainly contains five systems:

1. Excitation source system (electric field, through high voltage feedthrough, electron beam, for cathodoluminescence and UV-vis photons for photoluminescence);
2. Optical detecting system (PM system and CCD camera system);
3. Optical path controlling system;
4. Temperature controlling system;
5. Pumping system.

The excitation system and the optical detecting system are the core parts for luminescence measurements, while the other systems are auxiliary components.

The detecting system is composed by two parts according to the optical axis: optical axis No.1 is photoluminescence excitation source; optical axis No.2 a Peltier system cooled photomultiplier (PM) working in photon counting mode for integral light detection; optical axis No.3 a grating dispersive system (4.5 nm in resolution) coupled to a liquid nitrogen cooled charge coupled device (CCD) camera for spectral analyses which covers the wavelength range from 230 nm to 840 nm.

The core of this multi-purpose system is a light proof dark chamber connected to a turbo-molecular pump system to achieve high vacuum at  $10^{-4}$  Pa in order to avoid gaseous discharge during measurements. Samples can be placed on the holder which contact to a heating resistor, a nitrogen reservoir, and a temperature sensor, to control the temperature from liquid nitrogen temperature up to  $150^{\circ}\text{C}$ . The multi-purpose chamber is designed to accommodate different kinds of luminescence excitation. Picture of the system is given in Figure 2-4.

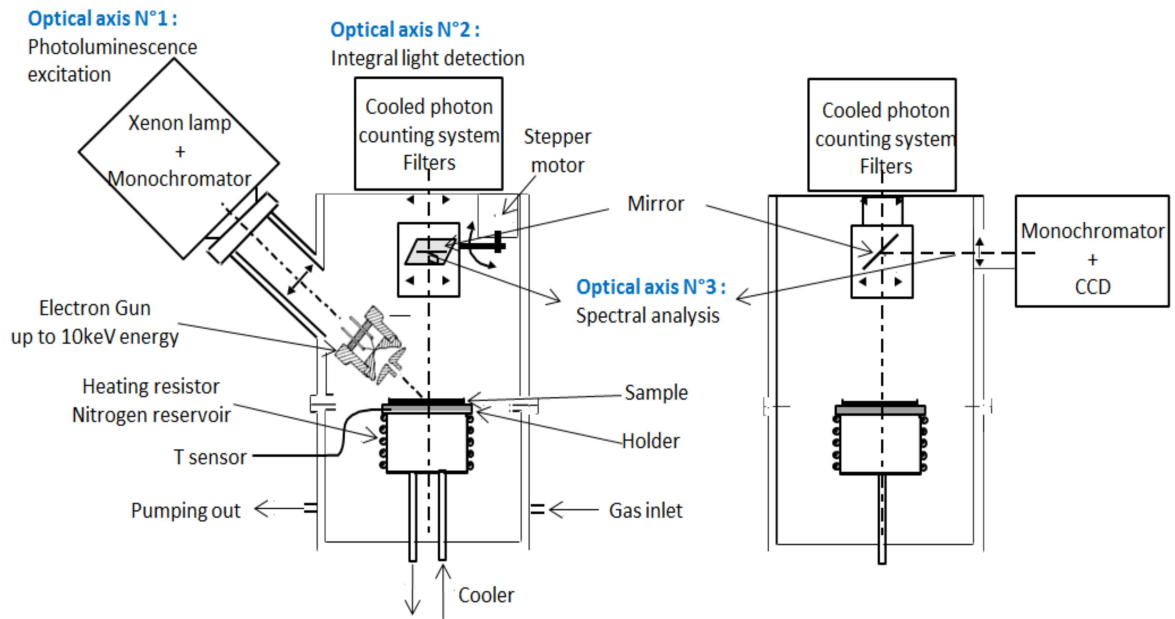


Figure 2 – 3: schematic of the multi-purpose chamber.

### a) Excitation source

In the system that we are introducing here, we can use three different types of excitation sources: **a) electric field excitation**, **b) optical excitation** and **c) electron beam excitation**.

The **optical excitation** is usually used during photoluminescence (PL) measurement, the sample mounted into the chamber at ambient atmosphere were excited by a xenon source coupled to an irradiation monochromator.

The **electron beam excitation** is used for cathodoluminescence (CL) measurement, a home-designed electron beam gun mounted into the chamber,

providing electrons of up 10 keV in energy. The filament is at negative high voltage and the anode at the ground.

However, in this dissertation we will mainly show results obtained previously by CL on PP films [58] and will compare these spectra to the newly acquired ones. New results are mostly with **electric field excitation**.



**Figure 2 – 4:** picture of the luminescence experimental setup.

During electroluminescence (EL) measurement, the configuration of Figure 2-5 was installed in the dark chamber and put under high vacuum. All the measurements are carried out at room temperature. Light detection can be carried out by two systems PM and CCD. The two electrodes HV tin electrode (inner diameter 30 mm) and ground flat electrode (diameter 40 mm) are connected to the high voltage and ground respectively. The ring electrode allows the light emission analyses from the centre of the sample.

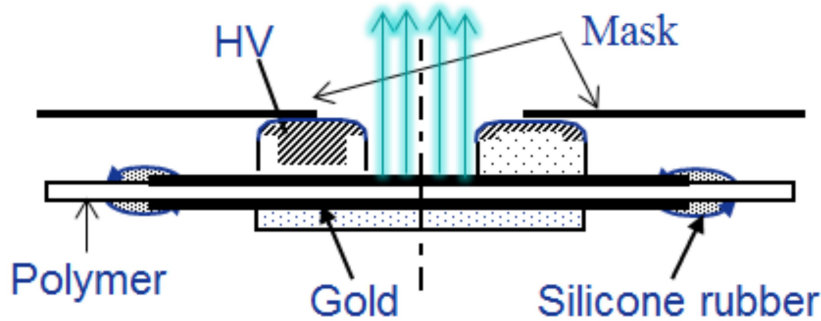


**Figure 2 - 5:** Configuration of EL measurement.

Direct current (DC), alternating current (AC) and pulse current (PC) can be applied to the dielectrics. In the figures here below are represented the AC and DC power supply systems. The AC power supply consists of an oscilloscope, a pulse/function generator and a high voltage amplifier up to 20 kV from Trek, Inc. USA. The amplification factor is 2000. Three kinds of AC voltage waveform (Sinusoidal, square and triangular) of AC can have been used to investigate the EL characteristics. The phase of AC voltage can be synchronized with the counting system which can archive the phase-resolved EL of the materials. The DC power supply is a 35 kV source from Fug, Germany. DC current is measured using a Keithley 617 programmable electrometer. With this equipment and PM system, the EL characteristics and current vs. field, phase-resolved EL, and spectra can be diagnosed. With CCD camera the spectra can be achieved under both DC and AC electric field.

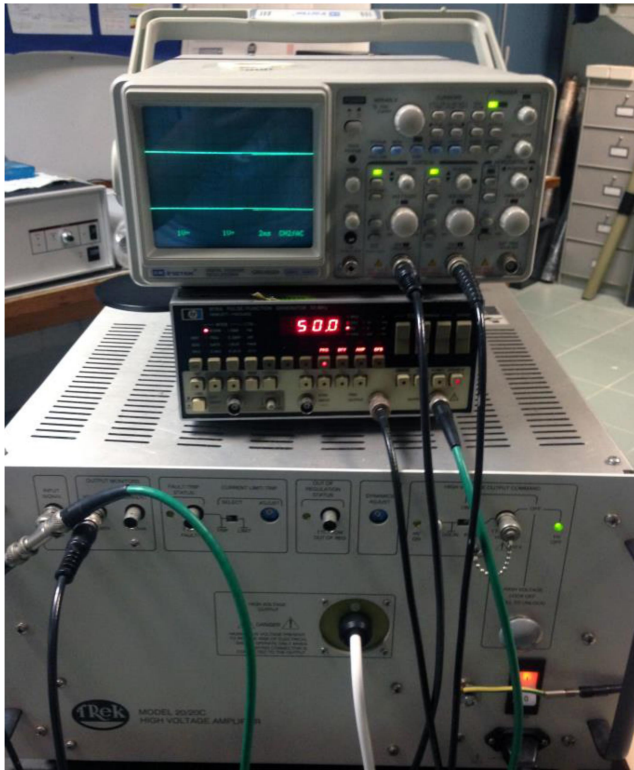


**Figure 2 – 6:** AC power supply. From top to bottom: an oscilloscope, a pulse/function generator and a high voltage amplifier. The amplification factor is 2000.

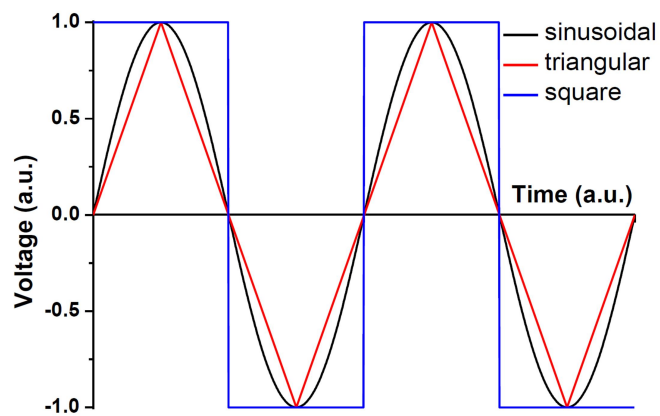


**Figure 2 – 7:** Three kinds of voltage waveform.

## **b) The photomultiplier detector – photons counting**

The photomultiplier (PM), type of Hamamatsu R943-02, as shown in Figure 2-8, is used to count photons emitted by the material. It allows observing resolved luminescence in time. It operates at a controlled temperature of  $-30^{\circ}\text{C}$  by a Peltier cooling system. This temperature has the effect of reducing the thermal emission of electrons from the photocathode, which implies extremely low noise (a few counts per second).

The signal transmitted by the PM is pre-amplified and then passes through a set of amplifier/discriminator and is finally transferred to a computer via a card of fast acquisition pulse counter from ORTEC. The integration time (dwell time) is variable from micro-seconds to several minutes. We used typically a counting dwell time of 2 s for recording EL-field characteristics and of  $1/200$  of the period ( $10\ \mu\text{s}$  for 50 Hz frequency) for recording EL phase resolved patterns.



**Figure 2 – 8:** The photomultiplier with cooling system of Hamamatsu R943-02.

## **c) The monochromator and CCD camera – spectra acquisition**

The CCD camera (Charge Coupled Device) from Princeton Instrument (LN/CCD-1100-PB) works at controlled temperature of  $-110^{\circ}\text{C}$ , cooled with liquid nitrogen. This camera is associated with an imaging spectrograph (type: Jobin-Yvon CP200) which ranges at 200 lines/mm. it covers a spectral range between 190 nm

and 820 nm. The sensitive part of the camera has a resolution of 1100 x 330 pixels, each covering an area of 24 x 24  $\mu\text{m}$ , summing information over the 330 rows. The spectral resolution is 4.5 nanometers. The CCD works either in spectral detection mode or in imaging mode. The output of the monochromator extends over the length of the detector at 1100 pixels, i.e. a point per 0.573 nm.



**Figure 2 – 9:** CCD camera with cooling system from Princeton Instruments (LN / CCD-1100-PB).

### 2.2.3 Plasma reactor description

In this section we will present the specific details of the plasma reactor used for nanocomposite synthesis.

The reactor used in this study exploits the plasma of an axially-asymmetric capacitively-coupled RF (13.56 MHz) discharge sustained at low gas pressure. It is illustrated in Figure 2-10. The axial-asymmetry of the discharge is related to the large difference between the surface area of the RF powered (upper) smaller electrode and the grounded (lower) electrode, including the reactor walls.

This type of discharges allows efficient sputtering from the powered electrode which in the current case is a silver target. The inter-electrode distance is of 35 mm. The RF electrode is coupled to a Sairem generator (delivered power up to 300 W) by means of a LC matching network. The axially-asymmetric design of that RF capacitively-coupled discharge produces axially-asymmetric plasma inducing a

self-bias voltage ( $V_{dc}$ ) on the powered electrode (the smaller electrode). The self-bias voltage scales up, in modulus, with the injected power in the discharge for a fixed gas pressure.

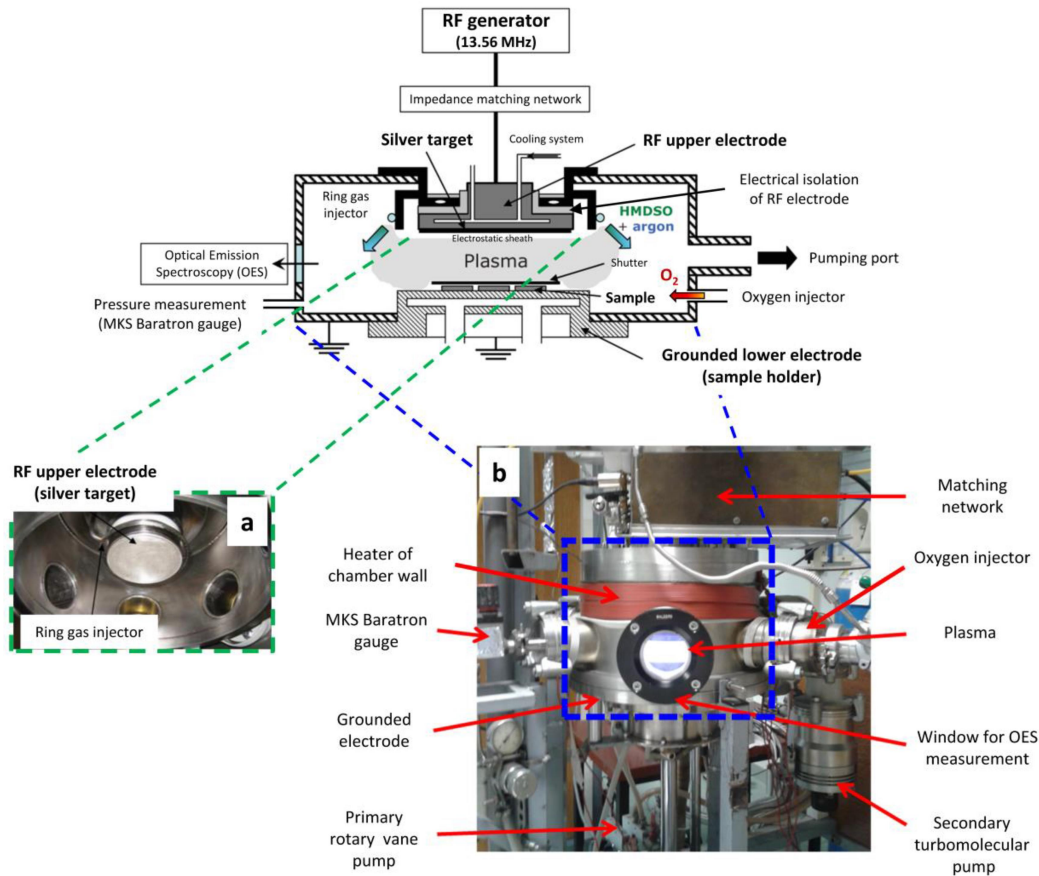


**Figure 2 - 10:** Schematic representation of the plasma reactor: (a) image of the inner upper part of the reactor chamber. (b) image of the reactor when the plasma is switched on.

The vacuum chamber is evacuated by a standard pumping system sustained of primary (rotary) and secondary (turbomolecular) pumps. Before performing the deposition the reactor is usually pumped overnight by the turbomolecular pump (down to  $5 \times 10^{-2}$  Pa). The working gas pressure is of few Pa. It is measured by a Baratron gauge. The operating gas used in this study is Ar (Air Liquide alphagaz 2, 99.9995%). As silicon precursor we have used hexamethyldisiloxane (HMDSO,  $[\text{CH}_3]_6\text{Si}_2\text{O}$ ) purchased from Sigma Aldrich (purity greater than 99.95%). The HMDSO line and the reactor walls are constantly heated at  $50^\circ\text{C}$  to avoid condensation of the HMDSO monomer. The purely technological interest of using HMDSO as precursor in plasma processing is maintained by the possibility of deposition of plasma polymers or thin oxide films (in HMDSO- $\text{O}_2$  mixture)

depending on the ratio of the partial pressures of injected gases. Furthermore, HMDSO is non-toxic, non-explosive, and much safer than silane.

One of the unique features of the experimental procedure is the pulsed injection of HMDSO with an injection time,  $t_{on}$ , and a total period,  $T$  ( $T = t_{on} + t_{off}$ ), see Figure 2-11. The maximum accessible HMDSO flow rate is 0.4 sccm, which actually corresponds to a continuous HMDSO gas injection. The HMDSO flow rate is adjusted by a mass flow controller OMICRON, switched by a pulse generator AGILENT.

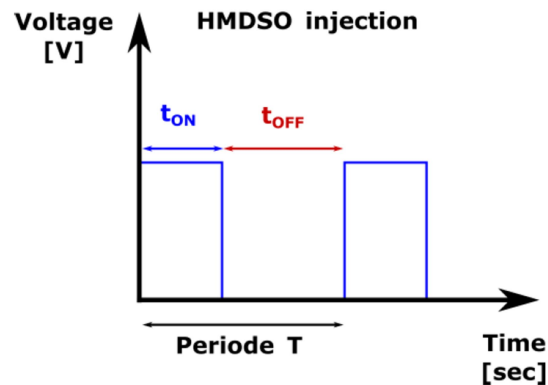


**Figure 2 - 11:** Illustration of duty cycle of HMDSO injection.

The Ar gas and the Ar-HMDSO mixture are introduced into the reactor by means of a ring gas injector located in the upper part of the reactor at the periphery of the RF electrode. The Ar and HMDSO are mixed in a buffer chamber before being injected in the reactor. A metallic shutter is positioned in the lower part of the reactor to hide the substrate during the plasma stabilization phase in order to prevent from continuous deposition on the sample once the plasma is switched on. It allows strict control over the deposition time.

The plasma electrical behaviour is followed through measurements of the self-bias voltage  $V_{dc}$ . The self-bias voltage of the RF electrode is at the origin of the acceleration of argon ions towards the silver target to achieve bombardment thus to the Ag-sputtering. The glow emission from the plasma is followed by Optical Emission Spectroscopy (OES). OES spectra are acquired through an optical fiber positioned at 5 mm above the grounded electrode, connected to a spectrometer Princeton Instrument (Acton Advanced Sp 2500A) for further analysis.

The plasma operating parameters are summarized in Table 2-3 for the sputtering step and in Table 2-4 for the plasma polymerization step.

Ag deposition conditions (sputtering step)				
Applied Power, $P$ [W]	Self-bias Voltage, $V_{dc}$ [V]	Ar pressure, $P$ [Pa]	Ar flow, [sccm]	Time, $t_s$ [sec]
80	- 940	5.2	2.8	5

**Table 2 - 3:** Parameters used to elaborate AgNPs by sputtering deposition process.

SiOC:H deposition conditions (plasma polymerization step)							
Applied Power, $P$ [W]	Self-bias Voltage, $V_{dc}$ [V]	Total Pressure, $P_{tot}$ [Pa]	Ar flow [sccm]	HMDSO injection time, $t_{on}$ [sec]	HMDSO period, $T = t_{on} + t_{off}$ [sec]	HMDSO average flow [sccm]	Time, $t_d$ [sec]
80	- 848	6.37	2.8	4	5	0.32	10

**Table 2 - 4:** Parameters used to elaborate the organosilicon SiOC:H layer.

Given the targeted architecture of the samples consisting of a stack of plasma SiOC:H/AgNPs layers on BOPP substrates the plasma deposited samples are

elaborated in two-step procedure: (1) Sputtering to deposit the AgNPs and (2) plasma polymerization to cover the AgNPs with a very thin organosilicon layer. All along the plasma process the BOPP samples are cooled to avoid any thermal induced damage. Moreover, the gas pressure, the self-bias voltage and the line intensity ratio are monitored during the plasma deposition process.

## 2.2.4 Monitoring of the plasma process by OES

The Optical Emission Spectroscopy is a non-contact diagnostic method largely applied for characterization of the main plasma parameters (electron energy and electron density) by means of measurements of the atomic optical transitions. The analysis consists of collecting light directly emitted by the excited species present in the discharge and further signal processing using theoretical models to describe the plasma [55].

In the plasma the glow emission occurs when species, atomic or molecular, in an excited energy (initial) level  $E_k$  totally or partially lose the acquired energy by a radiative decay mechanism (de-excitation) into a lower (final) energy level  $E_j$ , if the radiative transition between two energy levels is permitted. During this transition, a photon of wavelength  $\lambda_{kj}$  corresponding to the difference of the two energy levels is emitted. According to the Einstein relation of spontaneous emission the intensity of emitted light  $I_\lambda$  can be written as:

$$I_\lambda \propto \frac{hc}{\lambda_{kj}} N_k A_{kj}$$

where  $N_k$  is the population density of the initial excited level,  $A_{kj}$  is the transition probability between the energy levels  $k$  and  $j$ ;  $h$  and  $c$  being the Plank constant, and the speed of light in vacuum, respectively.

The most convenient way to use OES for real-time monitoring of a plasma process is to rely on the ratio between the intensities of two spectral lines. At steady state conditions it reads:

$$\frac{I_1}{I_2} = \frac{g_1 A_1 \lambda_2}{g_2 A_2 \lambda_1} \exp \left[ \frac{E_2 - E_1}{k_B T_e} \right]$$

where  $k_B$  is the Boltzmann constant,  $T_e$  is the mean electron energy and  $g_1$  and  $g_2$  are the corresponding atomic level degeneracies. The selection rules for a couple of emission lines are as follow:

- quite intense emission lines in order to collect a sufficient number of photons;
- high enough transition probabilities  $A$ ;
- emission lines with close to each other wavelengths.

In our plasma process, we follow the ratio between an argon emission line and a silver one. Both emission lines originate from highly excited atomic levels. It is important to estimate both the quantity of sputtered silver for the AgNPs deposition and the plasma efficiency for the elaboration of the plasma silica layers and the line ratio method appears the most appropriate one. For both deposition steps—sputtering and plasma polymerization—variation of the  $I_{Ag(546.6\text{ nm})}/I_{Ar(549.6\text{ nm})}$  ratio as a function of the injected power or the gas mixture composition was recorded. This kind of chart constitutes useful data to obtain reproducible results [43].

## 2.2.5 Ellipsometry

The ellipsometric spectroscopy is an optical technique commonly used in microelectronics for characterization of transparent thin layers, which enables to determine their optical and structural properties. The advantages of this technique involve its non-destructive and non-contaminant character. The sensibility of this technique to the structural changes is at nanoscale.

In this section, we present briefly the theoretical operation of ellipsometry. For more details about the technique refer to [56]. When an electromagnetic plane wave arrives on the flat surface of a sample, it can be transmitted, absorbed or reflected by this surface. The principle of spectroscopic ellipsometry consists in analysing the variation of two important parameters of the electric field of an electromagnetic wave, i.e. the amplitude and the phase, after reflection on the sample (Fig. 4-4).

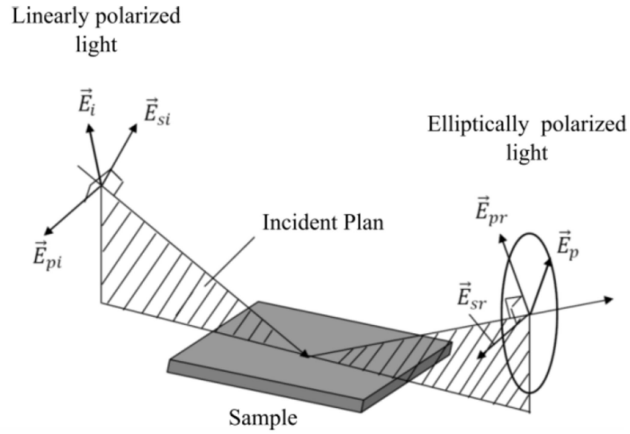


**Figure 4 - 4:** Schematic representation of the principle of ellipsometric measurement. The polarization of the incidence and reflected beam on the sample are marked.

The electric field of a polarized incident electromagnetic wave  $E_i$  is represented by two components: one with parallel,  $E_{pi}$ , and the other one with perpendicular,  $E_{si}$ , directions with respect to the incidence plane of the impinging beam. The two components ( $E_{pr}$  and  $E_{sr}$ ) of the electric field after reflection  $E_r$  on the sample surface undergo modifications that can be represented by the reflection coefficients of parallel,  $r_p$ , and perpendicular,  $r_s$ , polarization to the incidence plane as:

$$r_p = \frac{E_{pr}}{E_{pi}} = |r_p| e^{i\delta_p},$$

$$r_s = \frac{E_{sr}}{E_{si}} = |r_s| e^{i\delta_s}.$$

The real parts of these two complex coefficients ( $|r_p|$  and  $|r_s|$ ) represent the attenuation of the amplitude of the two electromagnetic wave components. The complex parts ( $\delta_p$  and  $\delta_s$ ) involve the phase change of these two components induced by the reflection. This provokes a change of the incident beam polarization (*i.e.*, from linear to elliptical polarization). Finally, spectroscopic ellipsometry measures the ratio of these two coefficients ( $\rho_e = \frac{r_p}{r_s}$ ) that depends on the wavelength of the incident beam.  $\rho_e$  can be written as:

$$\rho_e = \tan \Psi e^{i\Delta}$$

where  $\tan \Psi = |r_p|/|r_s|$  is related to the amplitude of the two electromagnetic wave components and  $\Delta = \delta_p - \delta_s$  is the difference of phase change of these two components after reflection. The measurement of  $\rho_e$  is performed by measuring the two quantities,  $\tan \Psi$  and  $\cos \Delta$ . Thus, measurement of these quantities at a fixed incidence angle as a function of the wavelength allows determining optical and structural properties of the sample by using different theoretical models.

In our study, the samples are composed of nanometric organosilicon layers elaborated on a silicon substrate that well reflects the light in the UV-visible-near infrared range. One or more parameters of each layer are unknown (refractive index –  $n$ , extinction coefficient –  $k$ , thickness of the layer). For interpretation of the recorded ellipsometry spectra modeling of the structure of these nanocomposites is required.

The spectroscopic ellipsometer used in this work is a Sopra GES 5 phase modulated system operating in the UV-visible-infrared range of the light spectrum from 0.2 to 2.8 microns (6.2 – 0.4 eV). This ellipsometer exploits the measurement method with rotating polarizer and fixed analyser. The advantage of this method is that measurements are not affected by the sensor sensitivity to the polarization.

# Chapter 3 Experimental results

## Synopsis

In the first part of this chapter, gold and ITO sputtered Polypropylene thin films are submitted to AC electric fields under vacuum, in conditions where gaseous discharges are avoided. This is very important to investigate emitted light from solid state material only, in the visible part of the optical domain. Phase-resolved EL is compared between different electrodes (gold and ITO).

In the second part we will investigate the impact of a new configuration of sample based on BOPP film on electroluminescence features through EL-field characteristics, spectral analyses and phase resolved EL under AC field. The new samples are characterized by a thin composite layer containing silver nanoparticles (AgNPs) deposited on the surface of Bi-axially Oriented Polypropylene. The idea is that this type of structure can enhance the emissions due to the Surface Plasmon Effect increasing the charge injection-extraction between the sample and the metallic electrode.

## 3.1 EL from reference structures

### 3.1.1 Samples

Measurements were carried out on BOPP films of 17.8  $\mu\text{m}$  thickness. These are “hazy” films with rough surfaces to promote impregnation of capacitors. Both surfaces of the film were metallized with semi-transparent layers of gold deposited by cold sputtering (thickness: 30 nm, diameter: 50 mm), or alternatively by sputtering transparent Indium Tin Oxide (ITO) layer (thickness: 135 nm, diameter: 50 mm) following the conditions described in Chapter 2. Observation of the film surfaces using an optical microscope in reflection and transmission mode has been achieved by B. Qiao et al. [54, 57]. Figure 3-1 clearly shows the differences

in roughness and transparency of the two surfaces, respectively, cf. Figure 3-1a and Figure 3-1b. In reflection mode and because of the small thickness of the films, it is not easy to distinguish features appearing on the both faces of the films (Figure 3-1 a and b). For this reason, films were gold-metallized providing pictures shown in Figure 3-1 c and d.

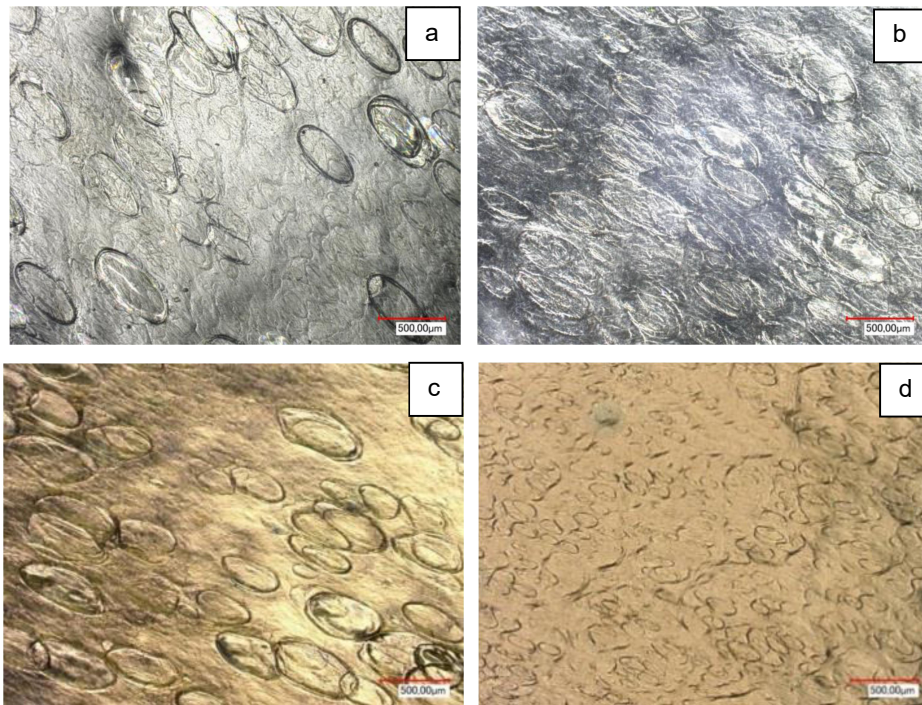


**Figure 3 - 1:** Optical microscopy of a: BOPP film from the rough surface, b: BOPP film from the smooth surface, c: Au-BOPP-Au from the rough surface, and d: Au-BOPP-Au from the smooth surface. Reflection mode. The red marks indicate a scale of 500  $\mu\text{m}$  [57].

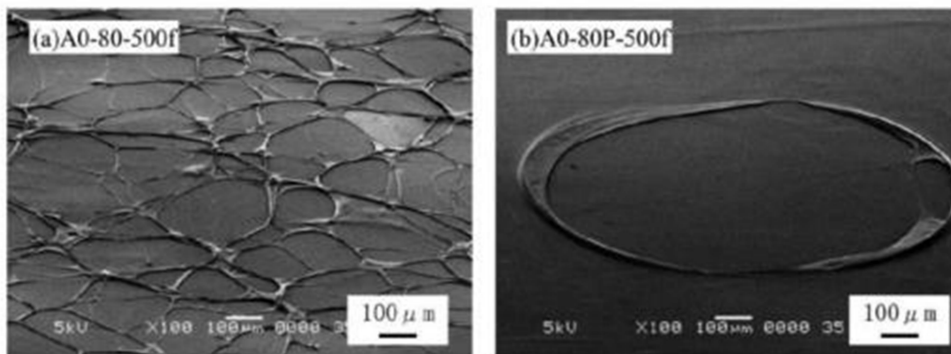


**Figure 3 – 2:** SEM image of the surface and the opposite side of BOPP sheet from [3].

It can be seen clearly from Figure 3-1 that there are elongated structures of different scale on each surface. Large (500  $\mu\text{m}$ ) and small (100  $\mu\text{m}$ ) crater-like structures define respectively rough and smooth surfaces. Their transmittance and thickness both vary in different film area, which is due to the physical structure of BOPP.

The morphology of BOPP films with crater-like structure have been reported in some studies since the 1980s. [58, 59] . We have estimated the depth of the craters to 2-3  $\mu\text{m}$  by optical microscopy.

In the SEM image we can clearly see that the depth of these structures formed during the stretching process of BOPP has a good relationship with the chill-roll temperature shown in Figure 3-4. The shape of the crater is closely related to the shape of crystal grains formed at the surface of BOPP [58].  $\beta$  crystals with lower density in PP sheet change into  $\alpha$  crystals with a higher density after stretching the sheet which contains both  $\alpha$  and  $\beta$  crystals. An explanation to the formation of crater-like surface roughness of BOPP films is based on the difference between the densities of  $\alpha$  and  $\beta$  crystals – however the complete mechanisms for crater formation are not yet fully elucidated [58, 59]. By the way, the crater structure is possible to design as it is required by controlling the trans-crystal structure in the surface layer of PP sheet. The thickness, roughness, density, and components of BOPP range at different regions of crater because of the crystal grain.

### 3.1.2 Protocols

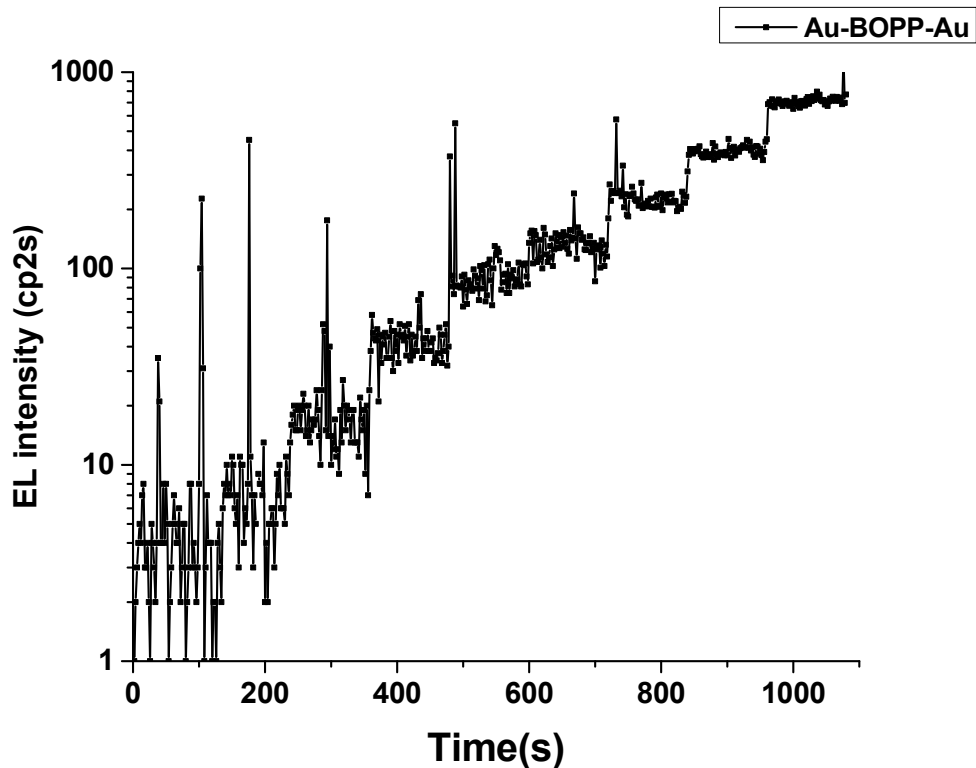
The measurements were archived under AC stress. The voltage delivered by the function generator was increased in steps of  $\Delta V = 200$  mV lasting 120 seconds. If we consider the amplification factor of 2000 supplied by the voltage amplifier and the thickness of the sample,  $s = 17.8$   $\mu\text{m}$ , the increase of field at every step is:

$$\Delta E = \frac{\Delta V \times 2000}{s} = 22.4 \text{ kV/mm}$$

Note that  $\Delta V$  and  $\Delta E$  above are defined as peak values, and so are all field values expressed in this work. The maximum field reached for this type of measurements,

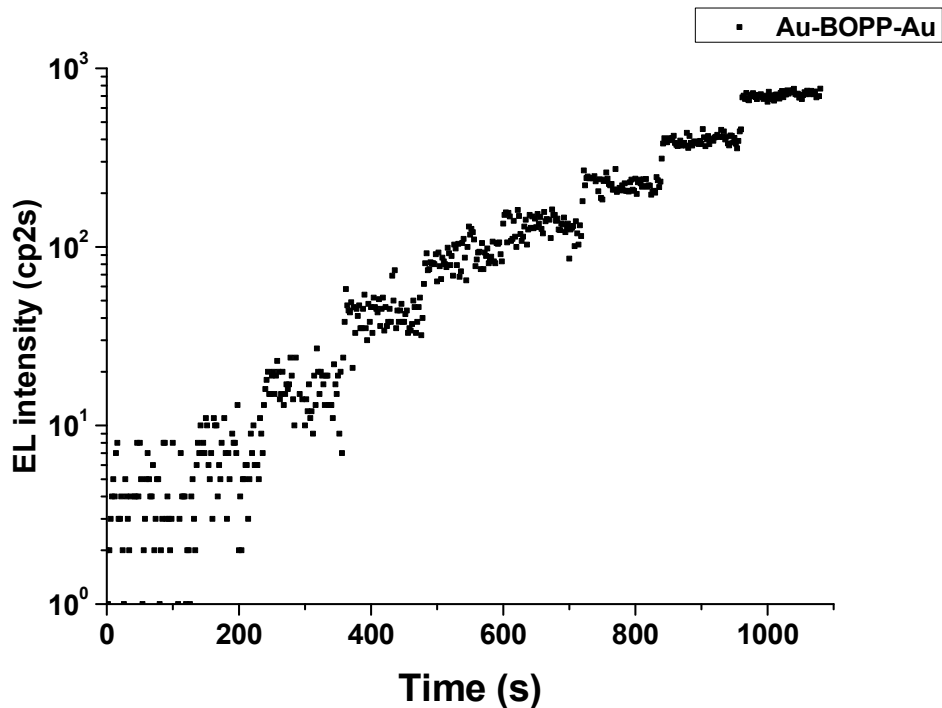
with samples composed by Au-BOPP-Au and ITO-BOPP-ITO, is 180 kV/mm. Several samples breakdown for fields often less than 100kV/mm; all results presented therein concern films having supported this maximum stress.

Figure 3-3 shows the rough results obtained for an Au-BOPP-Au sample with increasing the field in 9 steps up to 180kV/mm.



**Figure 3 - 3:** EL intensity vs Time for an Au-BOPP-Au sample. Before the data treatment we can see the presence of some points due to “noise” during the measurement.

Some noise clearly appears on the pattern and which is due to electromagnetic inferences. The occurrence frequency of noisy data appears not related to the applied field value, meaning that noise is related to electromagnetic inference in the ambient and not to discharge that could occur in the high voltage circuit. The signal has been denoised eliminating manually the data points exhibiting anomalous values; the result is shown in Figure 3-4.



**Figure 3 - 4:** EL intensity vs. Time for an Au-BOPP-Au sample after data treatment. Light intensity is given in photomultiplier counts per 2 seconds.

After the data treatment, in order to plot the EL intensity vs. Field, we have to average the EL intensity at every step. The results are shown in the next paragraph.

We repeat this kind of measurement applying an optical filter along the optical path of transmission spectrum of the photomultiplier with the intent of suppressing the red component emissions. The transmittance of the optical filter is shown in the Figure 3-5. It has a high light transmission rate in the wavelength range from 300 nm to 620 nm. In this way we can distinguish the contribution from the red emissions to the total signal.

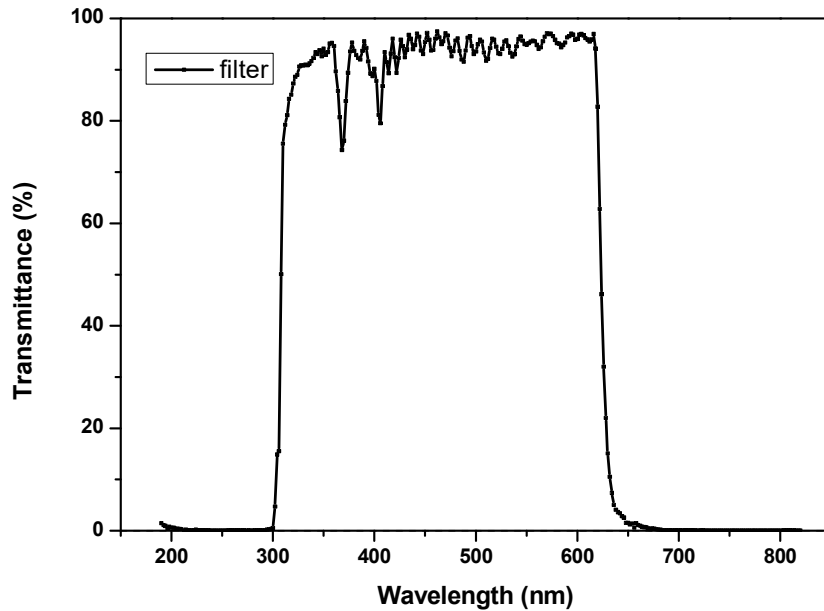


**Figure 3 - 5:** Transmittance of the 'red-censoring' filter.

Phase-resolved EL patterns were recorded resolving the phase of the AC signal into 200 segments and integrating the light for 400 seconds, i.e. for 2 seconds per segment. A synchronization signal is sent by the function generator at the beginning of the period of the HV signal and used as start of pass trigger for counting with the PM. The total integration time for each memory channel is of 2s. As the dwell time for each channel is set to 10  $\mu$ s (20ms of the AC signal at 50Hz divided by 200 segments), it means that the recording of a phase pattern is done cumulating the signal over 20000 periods. An example of "rough" Phase-resolved EL pattern is presented in Figure 3-6 before the data treatment for an Au-BOPP-Au sample under 180 kV/mm field. Here the time 0 is when voltage is at 0V on the rising side of the period and the stress is a sine AC stress.

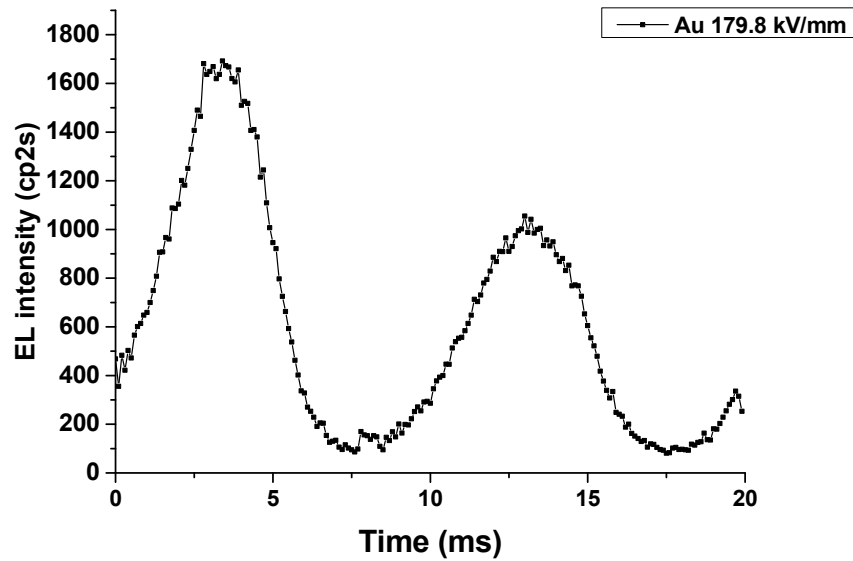


**Figure 3 - 6:**Phase-resolved EL pattern for Au sample before data treatment.

Here we can appreciate the real EL intensity level reached during the measurement, before the normalization process. To obtain the final results (cf. EL phase-resolved paragraph), we applied a smooth function to the curves (Savitzky-Golay) to best estimate the position (phase) of the peak.

### 3.1.3 Field dependence of EL under AC stress

Figure 3-7 shows the AC-Field dependence of light emission for AC voltage for Au-BOPP-Au sample.

The light intensity and the shape of the characteristics may vary from sample to sample, but there is a common feature in that the curves exhibit a typical upward convex shape in the low field region, that can be called “bump” for simplicity. This bump has already been reported and studied on different type of gold metallized polymer films under AC stress [23, 57].

As in previous studies, here we investigate how the “bump” in the EL-Field characteristics can be modified by using a low band path optical filter with enabling light detection with “red rejection”. It was shown that the red component emission contributes the “bump” in the EL intensity vs. field curve.

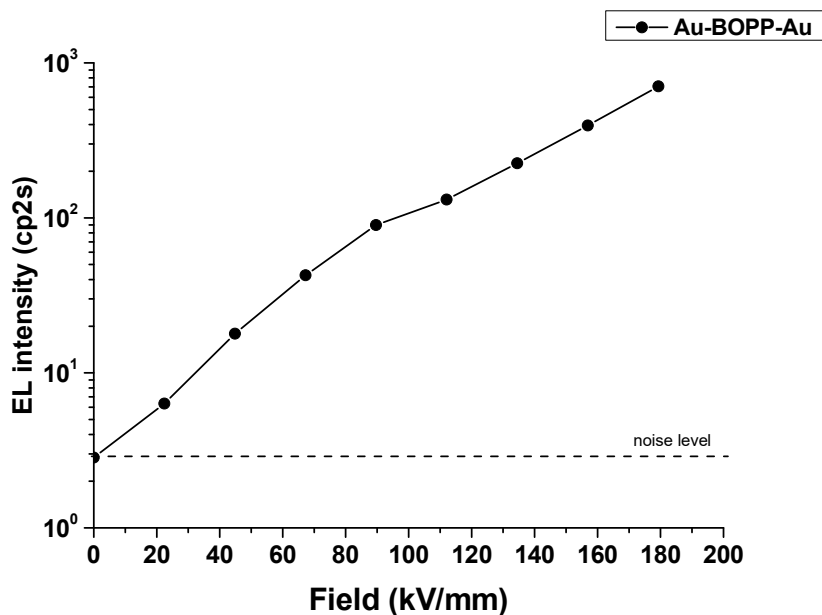


**Figure 3 – 7:** EL intensity vs field characteristics of Au-BOPP-Au under AC stress. The dotted line is the noise level of the measurement. Light intensity is given in photomultiplier counts per 2 seconds.

It is evidently shown that the “bump” of the EL vs field characteristic is associated with an emission in the red part of the spectrum and can be rejected by the filter as we can see in the Figure 3-8. This emission has been attributed in previous studies to the relaxation of Surface Plasmons excited by charge injection-extraction at the interface between gold electrodes and the dielectric material [23]. Surface Plasmons excited in metals can radiate light in the red part of the optical spectrum upon decay. A supplementary evidence of the involvement of Surface Plasmons was provided by the fact that the “bump” is not detected when using ITO electrodes. Such characteristic observed with ITO electrode is presented in Figure 3-9. It is evident how the EL emissions from ITO metallized samples are lower at low Field compared to gold samples, but as the field grows the difference between the two characteristic decreases. This seems to confirm the idea that the relative contribution of the red emission decreases as the electrical field is increased.

The EL-field characteristic of BOPP with ITO electrodes present the same shape as that with Au electrodes and red-filtering, confirming that the “bump” is due to red component emission, presumably due to Surface Plasmon effect of the Au electrodes.

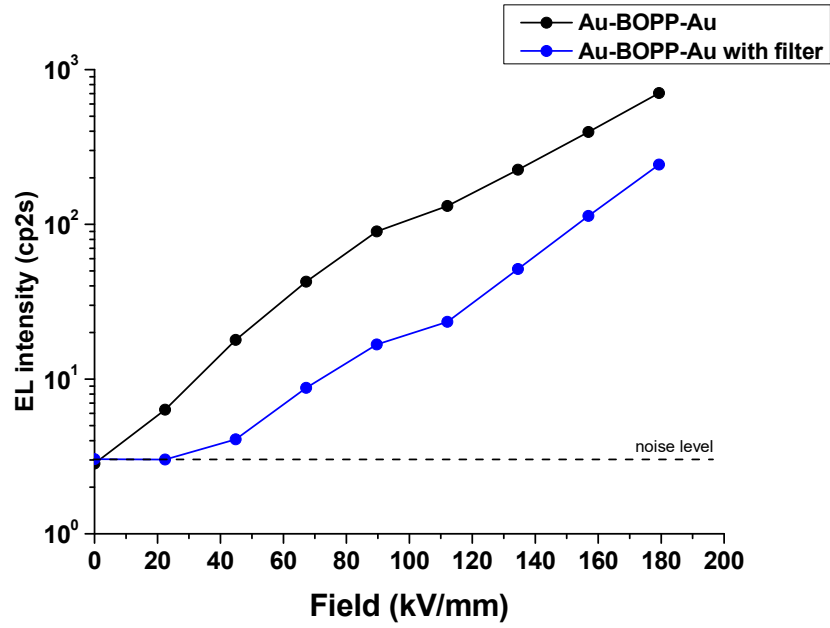


Figure 3 – 8: EL intensity vs field characteristics of Au-BOPP-Au with and without red-censoring filter under AC stress.

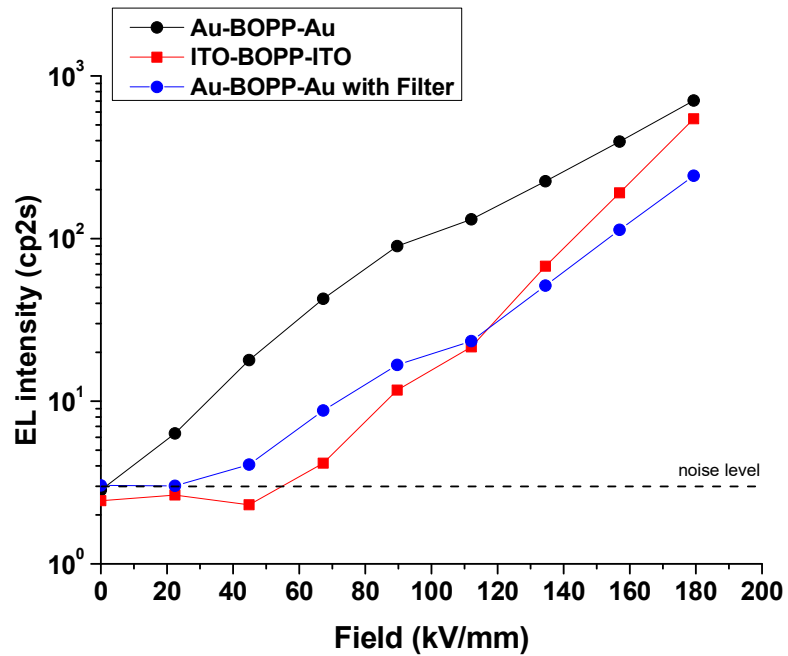


Figure 3 – 9: EL intensity vs field characteristics of Au-BOPP-Au with and without red-censoring Filter and ITO-BOPP-ITO under AC stress.

With the large steps in field used here, it is not easy to define a precise threshold field for light emission. For the characteristic with gold electrodes as in Figure 3-7, the light level is important already for the first step at 20kV/mm. When removing the components (through filtering in case of Au electrodes, or with using ITO electrodes, the threshold field would appear in the range 20 to 40kV/mm. The question of threshold for EL under AC stress is not easy to unravel as the apparent threshold may be set up sensitivity-related emission. Alternatively, it may define the field level under which no excitation of the material is provided, i.e. a physical threshold for the material. In [23], it appeared that the EL-field characteristics, excluding the red component, for several polymers tend to show a functional dependence as a Schottky law, i.e.  $EL\% \exp(\alpha E^{1/2})$ , already for an applied field of a few kV/mm. This would mean that the threshold is essentially sensitivity limited.

### **3.1.4 Phase resolved EL under AC stress**

With the purpose of investigating the relationship of EL intensity and curve with voltage waveform, here we present some examples of phase-resolved EL measurements.

In Figure 3-10 we have represented in black the “rough” phase pattern of an Au-BOPP-Au sample for a field of 112.4 kV/mm and in red we have superimposed the smoothed signal obtained with a Savitzky-Golay function with 32 points of windows and polynomial order of 3. The smoothed curve represents a fair reproduction of the envelope of the rough signal and at the same time allows an easy extraction of quantitative parameters for the patterns such as phase and amplitude of EL peaks along with width of the peaks.

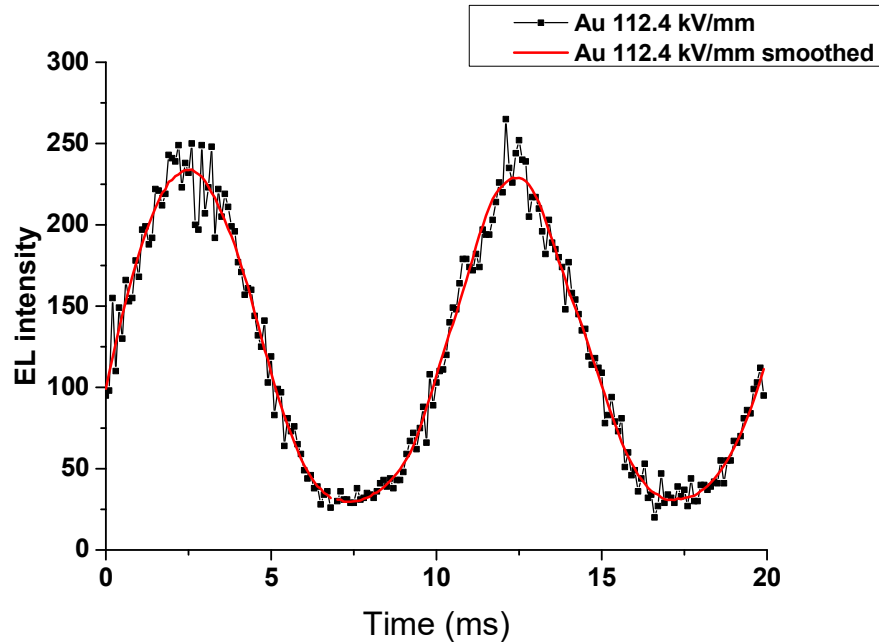


**Figure 3 - 10:** Phase-resolved EL of BOPP films under 50 Hz AC stress. Before and after “smoothing” process

#### a) Phase patterns with Au Electrodes

In Figure 3-11 we have superimposed the EL phase patterns obtained at two different fields. Figure 3-12 compares the patterns obtained with and without red-censoring filter (same sample used in all cases), for the same applied field. The voltage waveform is given to the top of the figures. Looking at the general form of all patterns, we can notice that the signal is always in advance if we compare it with the voltage sign. This result has been reported in the past [60], but the most striking result we obtained here is a substantial difference in the shift depending on the field level and on the presence of the filter.

With increasing the field, the EL appears more in phase (cf. Fig. 3-11). Looking at Figure 3-12, we also have a clear impact of the filtering on the phase shift: without filter, the response appears more in phase. These two features clearly indicate that bulk emission and red emission have distinct phase patterns.

Another remarkable fact is the dissymmetry in the amplitude of the EL peaks detected under positive and negative voltages when using the red filters. This might also be related to the non-symmetric topology of samples surface for example.

In Figure 3-13 we present the evolution of the EL phase-resolved pattern (without filter) for different fields in an Au-BOPP-Au sample, before and after normalization. It is clear that the EL is more in-phase as field is increased. We can also notice that the ratio of the intensity of the peaks under positive and negative half-cycles changes as a function of field, being more di-symmetrical with increasing field.

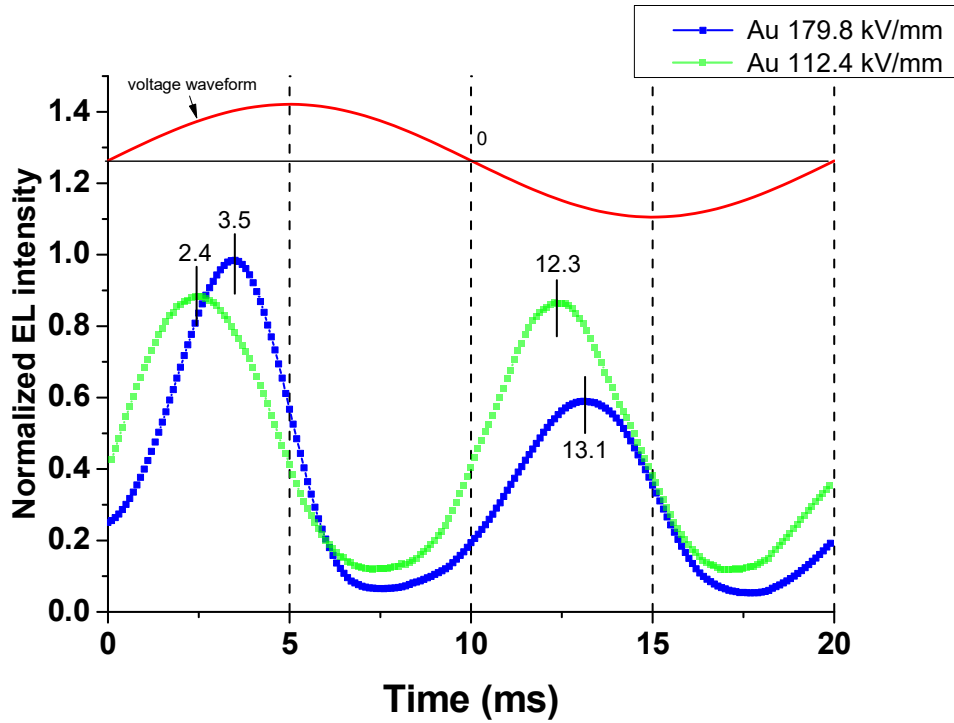


**Figure 3 – 11:** Phase-resolved EL of BOPP films under 50 Hz AC stress. Light intensity is normalized to 1 in the second half period. Same sample Au-BOPP-Au at different fields.

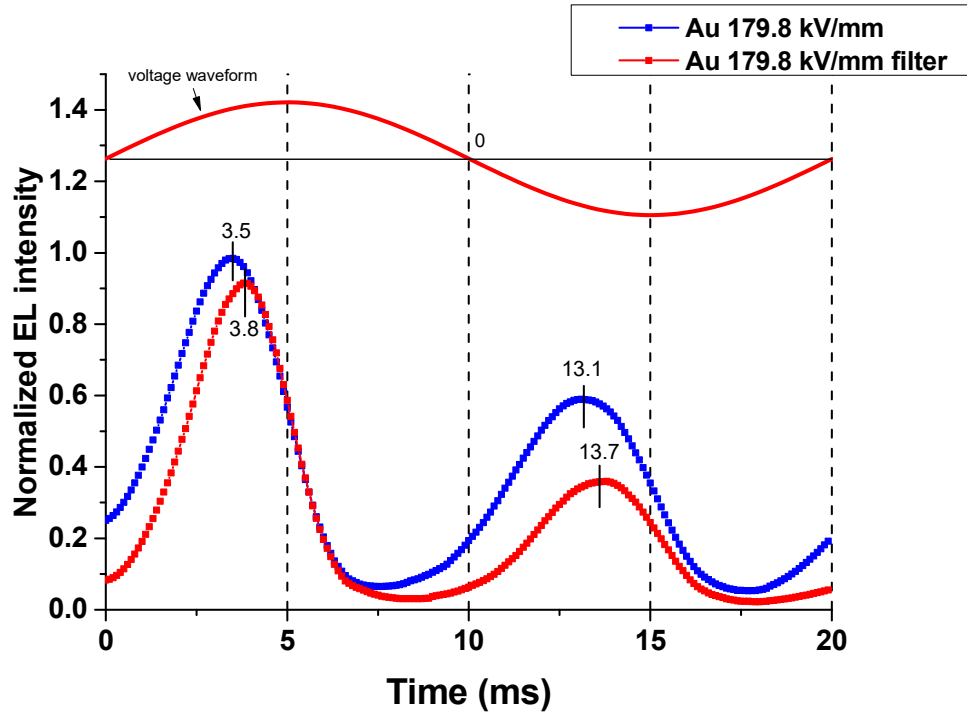
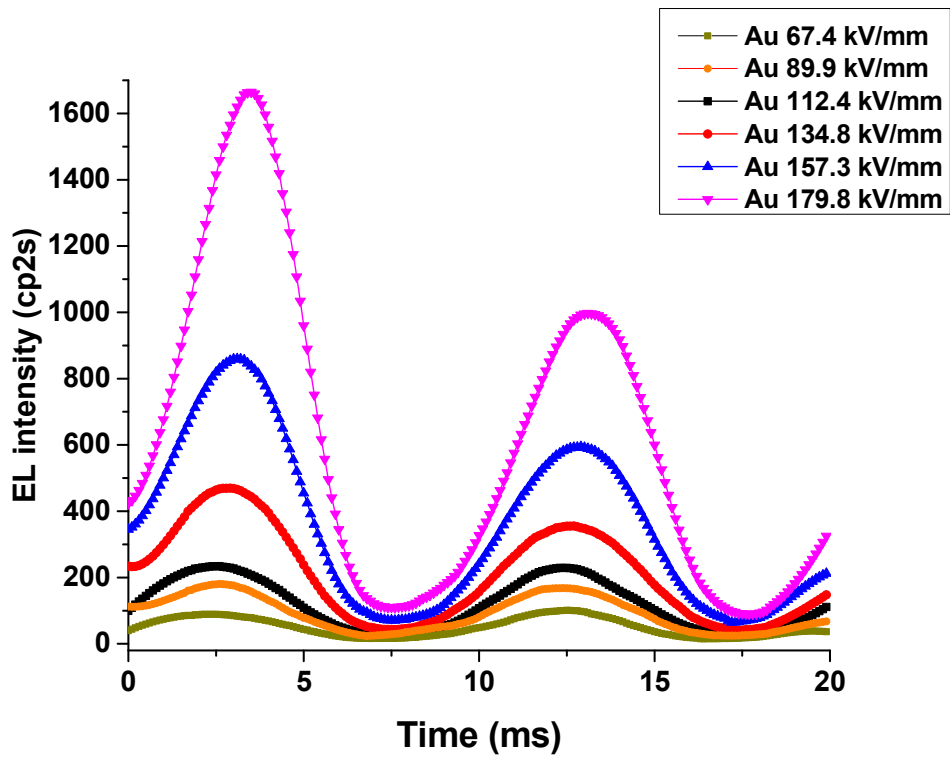
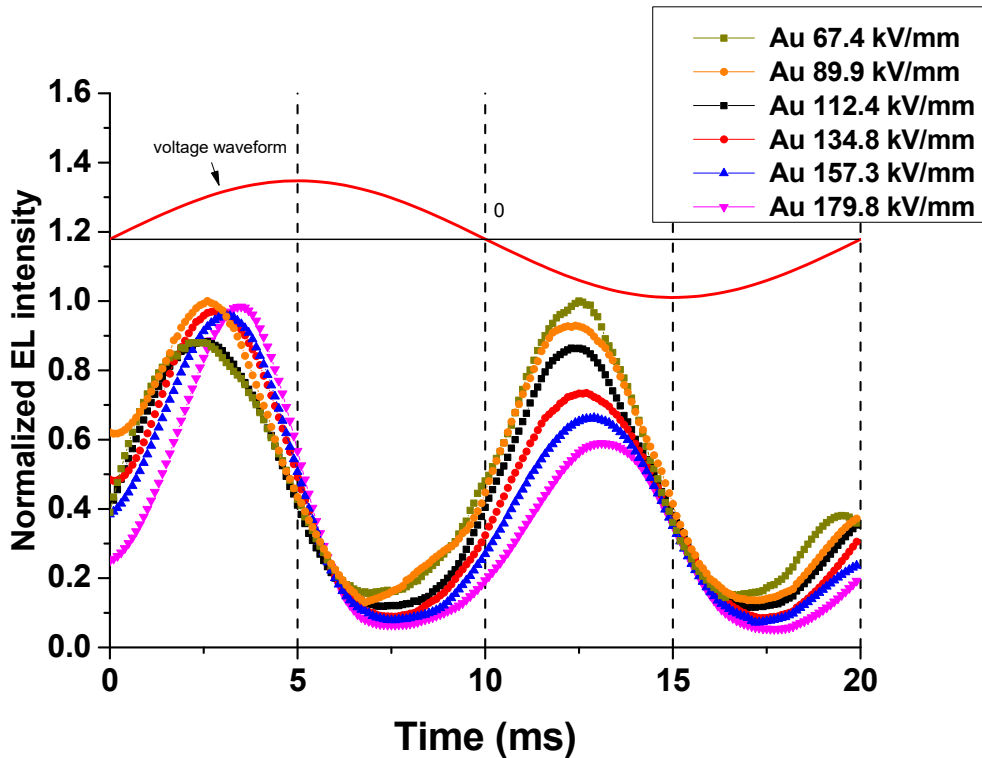


Figure 3 – 12: Phase-resolved EL of BOPP films under 50 Hz AC stress. Light intensity is normalized to 1 in the second half period. Same sample Au-BOPP-Au with and without filter.



(a) before normalization



(b) after normalization of light intensity to a maximum value of 1.

**Figure 3 - 13:**Phase-resolved EL of BOPP films under 50 Hz AC stress. Same Au-BOPP-Au sample at different fields.

### b) Phase patterns with ITO Electrodes

Figures 3-14 and 3-15 show the EL phase patterns in case of ITO electrodes considering respectively field effect and the impact of filtering. A priori there is no reason to expect an effect of the filter in case of ITO electrodes since ITO does not exhibit plasmon resonance in the visible range. Besides, it was confirmed by the acquisition of the EL spectrum of ITO-metallized PEN samples that there is no contribution in the red domain [58].

The patterns are rather dissymmetrical, considering amplitude as well as phase angle. Possibly the data for the positive half-cycle are not fully reliable- see also Table 1 for the large variation in phase values. Considering the main peak (under half period with negative voltage), the position remains nearly unchanged. One can wonder if the phase could be independent from the field when no plasmon can be radiated (even with filtering, not necessarily all the light resulting from SP excitation is removed).

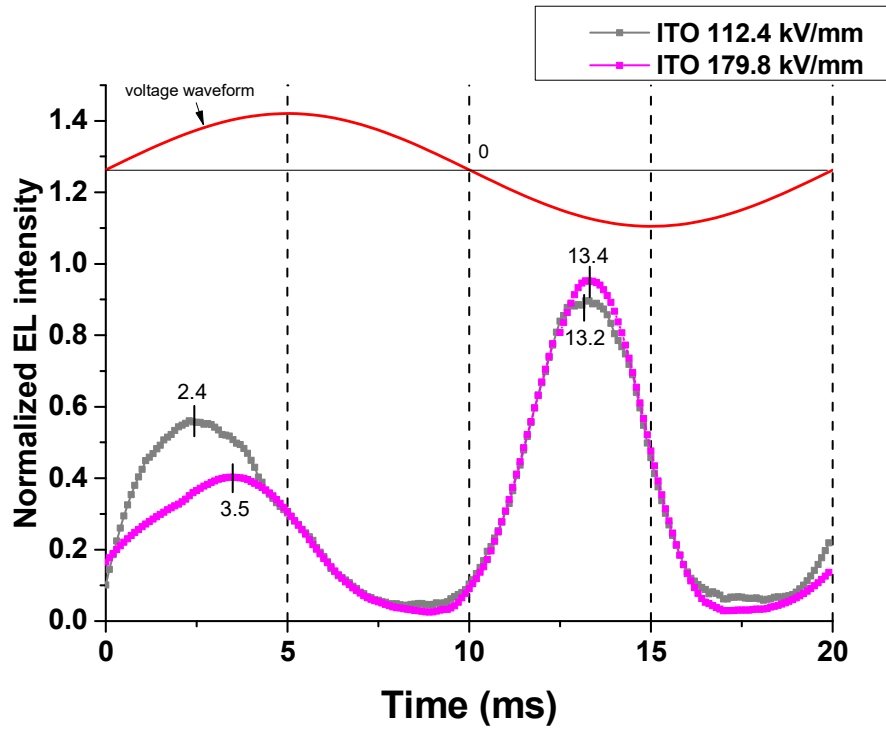


**Figure 3 – 14:** Phase-resolved EL of BOPP films under 50 Hz AC stress. Light intensity is normalized to 1 in the second half period. Same sample ITO-BOPP-ITO at different fields.

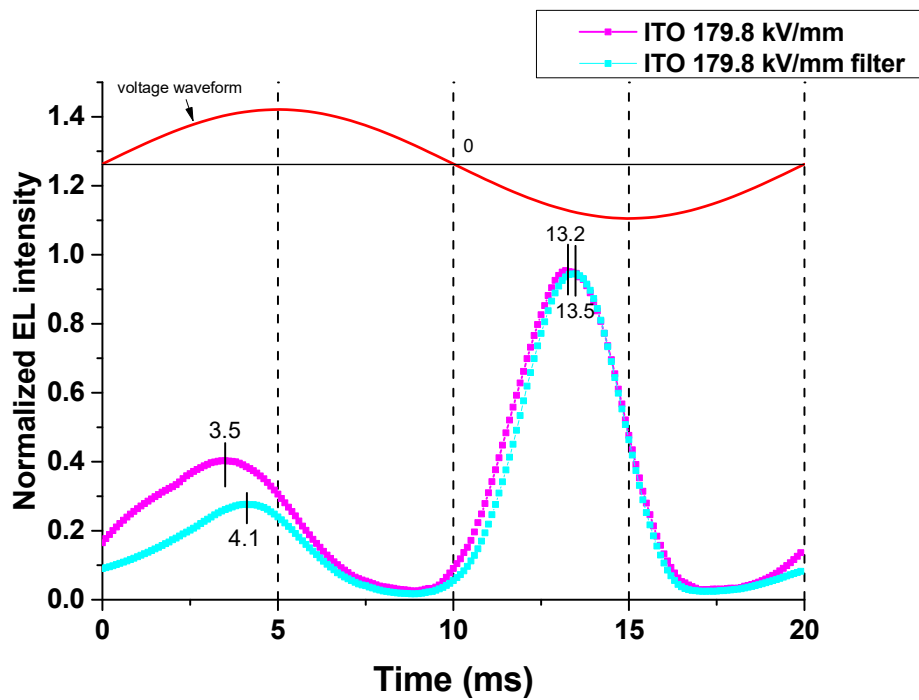


**Figure 3 – 15:** Phase-resolved EL of BOPP films under 50 Hz AC stress. Light intensity is normalized to 1 in the second half period. Same sample ITO-BOPP-ITO with and without Filter.

### 3.1.5 Discussion

In Table (3.1) we reported, for every curve we obtained, the amplitude, the FWHM (Full Width at Half Maximum) and the phase, defined as the angle (in degree) between the voltage peak and the EL peak. We divided the table in two parts, positive half period and negative half period. Some of the features previously addressed are clearly revealed such as the progressive decrease of the phase angle with increasing the field, the effect of the red filter in reducing the phase angle (for Au electrodes), and in general the relative low angle when no red component is present. In general, the peaks are narrow (smaller FWHM) when the phase angle is small tending to single emission process as opposed to distributed processes.

Peak at:			Positive Half Period			Negative Half Period		
Field	Electrode	Filter	Phase (°)	Amplitude (Cp2s)	FWHM (ms)	Phase (°)	Amplitude (Cp2s)	FWHM (ms)
67.4	gold	no	45.0	91	4.8	48.6	103	4.9
89.9	gold	no	39.6	180	4.7	48.6	175	4.6
112.4	gold	no	45.0	232	4.7	46.8	228	4.7
134.8	gold	no	37.8	469	4.8	41.4	355	4.8
157.3	gold	no	34.2	859	4.5	37.8	594	4.7
179.8	gold	no	27.0	1664	3.8	34.2	997	4.6
112.4	gold	yes	27.0	55	4.3	34.2	31	4.7
179.8	gold	yes	21.6	971	3.2	21.6	382	4.3
89.9	ITO	no	39.6	59	4.0	34.2	88	3.5
112.4	ITO	no	41.4	89	4.6	34.2	144	3.6
134.8	ITO	no	23.4	175	5.6	32.4	412	3.4
157.3	ITO	no	28.8	388	5.3	32.4	980	3.4
179.8	ITO	no	27.0	506	5.5	32.4	1192	3.5
112.4	ITO	yes	12.6	25	4.7	21.6	65	3.1
179.8	ITO	yes	16.2	398	4.7	27.0	1360	3.3

**Table 3 - 1:** Sum-up of characteristics of EL phase patterns obtained with gold and ITO electrodes.

The EL intensity of BOPP films under AC stress is relatively high because the alternative voltage produces injection of charges of alternating polarity into the material. Comparatively, under DC stress, the EL from BOPP was of a few cp2s [61] even for fields beyond 300kV/mm. It is interesting to note that with the increase of the electric field the EL increases nonlinearly with a threshold at a certain electric field of less than 10 kV/mm in case of Au electrodes and higher for the ITO (40 kV/mm).

As stated above, the most straightforward and probable excitation mechanism for EL under AC, for insulating polymers, is that involving charge recombination. Hence, EL under AC appears as a near-electrode effect, charges injected under one polarity in a given half-cycle of AC stress recombine with previously injected charges of opposite polarity during the previous half-period of stress. The description is somewhat substantiated by modelling of EL as a function of the AC waveform (square, triangle, sine, with or without offset) and voltage offset based on bipolar charge injection, trapping and recombination.

Indeed, to better understand what happens during phase-resolved EL measurements in insulating polymers, in this case polyethylene, but can be applied also to BOPP, in the literature Baudoin *et. al.* [61, 62] simulated the phase resolved EL, based on charge injection, transport and recombination model. A hopping mobility of electronic carriers between traps with an exponential distribution in depth was used.

During one cycle of sinusoidal waveform voltage there are several steps for charge transport, trapping, de-trapping, and recombination processes as depicted in Fig. 3-16.

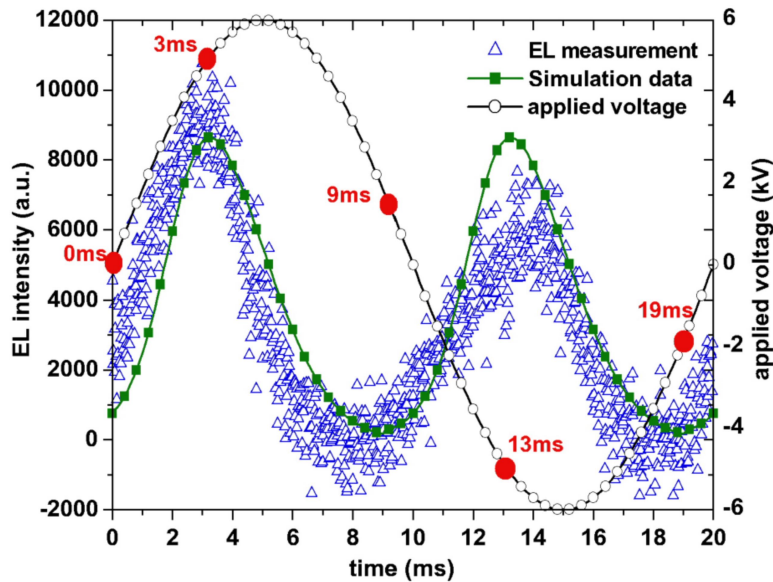


**Figure 3 – 16:** Comparison between EL measurement and simulation under sinusoidal waveform [1]

- At  $t = 0$  ms (under zero applied voltage), electric field at the reference electrode is negative (because the net density of charge is positive due to the previous accumulated positive charge within the positive half cycle) and hence electrons begin to be injected and holes begin to be extracted. Injected electrons are then trapped and some of them recombine with trapped holes: hence, the recombination between injected electrons and trapped holes increases in time.
- At  $t = 3$  ms, electric field at the cathode, recombination rate, injection current for electrons and extraction current for holes are practically at their maximum. The net density of charge begins to be negative (in the first cell, charge is negative) and the electric field at the cathode reaches progressively the applied field.
- Between  $t = 3$  ms and  $t = 9$  ms, negative carriers are majority carriers in all the cells close to the cathode and this homocharge induces a lowering of the applied field. In this time interval, the recombination rate between injected electrons and trapped holes decreases, i.e. the EL intensity decreases.
- Between  $t = 9$  ms and  $t = 13$  ms, the electric field at the reference electrode is positive, positive carriers are injected but the net charge density remains

negative, acting as an heterocharge that enhances the electric field at the reference electrode relative to the applied field. The recombination between injected holes and trapped electrons begins to increase.

- At  $t = 13$  ms, the electric field at the reference electrode, recombination rate, injection current for holes and extraction current for electrons are practically at their maximum. The net density of charge begins to be positive (in the first cell, charge is positive) and the electric field at the electrode reaches progressively the applied field. As previously, this feature appears before the maximum of the applied field.
- Between  $t = 13$  ms and  $t = 19$  ms, positive carriers are still injected (positive electric field at the electrode) and reduce the electrode field. Injection current for the holes decreases and hence the recombination between injected holes and trapped electrons decreases.

An interesting aspect of the model is its capability to reproduce the advance of phase. Of course the EL is supposed to be related to the density of recombination of carriers - electrons and holes. During this process, the energy is released through radiated light but there can be parallel relaxation processes through chemical pathway initiating electrical ageing [63, 64]. Interestingly, according to the model the recombination rate, injection current for one type of carriers and extraction current for the opposite polarity carriers are practically at their maximum at the same time: this means than other light excitation processes than charge recombination, linked for example to injection current can also explain the EL features. Plasmon-related emissions are supposedly related to the current and such process remains consistent with the model.

With the model it was shown that the charge recombination would occur in a region within a few nm from the electrode [62]. Therefore, all possible excitation mechanisms for EL are in a region very near to the electrode.

To sum-up, considering first phase-resolved EL, the phase advance will decrease along with the increase of electric field. The crest of EL intensity is the crest of recombination of charge carriers.

The injected electrons recombine with the residual holes injected during last period, which makes the crest of recombination in advance of applied voltage. The

electrode is another factor that affects the advance of the phase of EL under AC stress. The red component emission contributes strongly to the intensity at low AC electric field. The model could account for plasmon-related effect supposing that excitation is directly related to extraction/injection processes. The red component emission makes the EL crest in EL phase pattern advanced due to its relative strong intensity at low field. Hence, the EL intensity is a sum of both light from material itself and from the red component emission.

### **3.2 AgNPs tailored BOPP: structure and EL characterisation**

In this section, our aim is to report on the electroluminescence features of a new type of BOPP sample with substantially modified interface conditions. Investigations are achieved through EL field characteristics, spectral analyses and phase resolved EL under AC field. The new samples are characterized by a thin composite layer containing a single layer of silver nanoparticles (AgNPs) deposited on the surface of Bi-axially Oriented Polypropylene (BOPP) and covered by a very thin organosilicon layer. The idea is that this type of structure can enhance the emissions due to the Surface Plasmon effect increasing the charge injection-extraction between the sample and the metallic electrode. As such a composite layer [70] was shown to be efficient plasmonic structure we used the idea here to distinguish the respective role of processes due to charge recombination and those related to surface plasmon radiation.

Part of electroluminescence phenomena presented in the last section has been attributed to SP emission in insulating polymers with noble metal electrodes (Au). SP processes do not seem to be present in Indium Tin Oxide (ITO).

### 3.2.1 Sample preparation

The nanocomposite layer is synthesized in a low pressure plasma reactor enabling sputtering from a silver target and a plasma polymerization of hexamethyldisiloxane (HMDSO— $[\text{CH}_3]_6\text{Si}_2\text{O}$ ) as two independent steps in the same plasma chamber.

To accomplish deposition of multifunctional layers we have used an axially asymmetric RF (13.56 MHz) capacitive coupled discharge maintained at low gas pressure (40 mTorr = 5.2 Pa). The plasma reactor is described in Chapter 2. Here we briefly remind the principle of operation of this plasma process.

The RF-driven top electrode (smaller, 10 cm in diameter) was placed in front of a bottom electrode (larger, 12 cm in diameter) with a gap distance equals to 3.5 cm. The bottom electrode and the walls were grounded. Furthermore the bottom electrode is water cooled, this particular is very important, because during the deposition, in the chamber, we can reach high temperature that can damage our sample, in fact BOPP is a heat-sensitive material.

The axially asymmetric design of the RF discharge produces axially asymmetric plasma inducing a self-bias voltage ( $V_{dc}$ ) on the powered electrode. The self-bias voltage results from the DC voltage drop between the bulk plasma and the electrodes across the plasma sheaths connecting the driven electrode to the ground. It is negative in the usual case. Since the voltage drop across the sheaths is inversely proportional to the sheaths capacitances, the sheath with smaller area (smaller electrode) has smaller capacitance inducing thus higher self-bias voltage scales up, in modulus, with the injected power, at a constant pressure and is at the origin of the acceleration of Argon ions towards the silver target to archive bombardment. The most appropriate way to follow the plasma behaviour in order to relate it to the plasma glow emission as the line intensities increase with either the electron energy or the electron density. Figure 3-17 represents an optical emission spectrum of the plasma glow emission during the sputtering step. The evolution of line intensity ratio of  $I_{\text{Ag}(546.6\text{nm})}$  to  $I_{\text{Ar}(549.6\text{nm})}$  gives an image of the Ag-amount in the plasma which is related to the Ag-volume fraction deposited on the substrate; the higher the line intensity ratio, the higher the Ag-volume fraction is. The variation of the line intensity ratio ( $I_{\text{Ag}(546.6\text{nm})}/I_{\text{Ar}(549.6\text{nm})}$ ) as a function of the

injected power or the gas pressure is recorded for each deposition. A set of charts is created during the plasma diagnostic phase that later on is used during the deposition process as it constitutes useful data to obtain reproducible results. More details on the plasma process can be found in references [19, 43, 51].

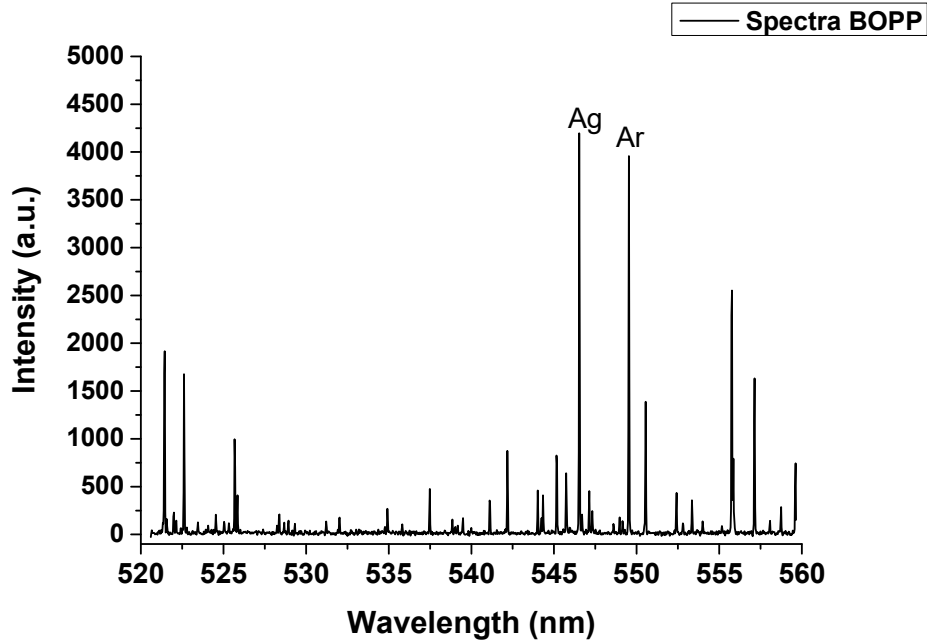


**Figure (3.17):** Optical Emission Spectrum of the plasma during the AgNPs layer deposition. The two spectral lines used to control the amount of silver during the plasma deposition are  $I_{\text{Ag}(546.6\text{nm})}$  and  $I_{\text{Ar}(549.6\text{nm})}$ .

The deposition was performed in two-step process: first the silver layer (AgNPs) is sputtered followed by plasma polymerization to create the dielectric cover matrix. To prepare our samples the sputtering time is 5 s with a plasma maintained in pure Argon at pressure of  $p = 5.2$  Pa with the RF power of  $P = 80$  W ( $V_{\text{dc}} = -940$  V). The dielectric layer is obtained in same reactor with argon-hexamethyldisiloxane (HMDSO,  $[\text{CH}_3]_6\text{Si}_2\text{O}$ ) mixture at a total gas pressure of  $p_{\text{tot}} = 6.37$  Pa, input power  $P = 80$  W ( $V_{\text{dc}} = -848$  V).

The BOPP samples are hidden behind a shutter for the time of plasma process stabilization and then exposed to the plasma during the deposition time by removing the shutter. It allows controlling the short deposition times used to this experiment.

In order to complete the multifunctional layer we sputtered, on both sides of the sample, a thin layer of ITO (125 nm), this will be the stratum in contact with the electrode during the EL measurements, cf. Figure 3-18.

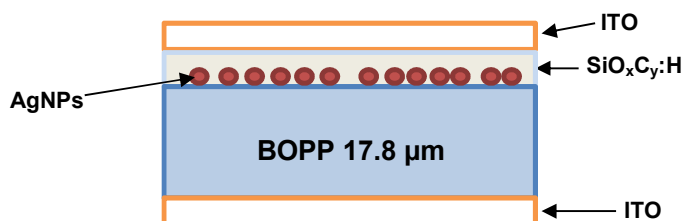


**Figure 3 - 18:** Structure of the multi-layer sample (ITO-BOPP-AgNPs- SiO<sub>x</sub>C<sub>y</sub>:H-ITO).

### 3.2.2 Physico-chemical characterization of the composite layer

The formation of metallic nanoparticles during plasma sputtering depends strongly on the plasma operating conditions and reactor geometry but also on the used substrate. The substrate can influence the organisation of the nanoparticles by roughness or by available active bonds on the surface. Figure 3-19 shows Scanning Electron Microscopy (SEM) images of a single layer of AgNPs deposited for the same plasma operating conditions in the plasma reactor described in Chapter 2 on silica (SiO<sub>2</sub>) layer (Fig. 3-19(a)) and on low density polyethylene (LDPE) (Fig. 3-19(b)). Although the two substrates are different; the SiO<sub>2</sub> surface is apolar, presenting many –OH bonds and the LDPE-surface is polar, the main difference in the organisation of the obtained AgNPs stems from the surface roughness, only 1 nm for the SiO<sub>2</sub> and in the micrometer range for the LDPE. The mean size of AgNPs is of 20.0 nm with larger size distribution for the polymer substrate ( $\pm 10.0$  nm). The mean surface density of AgNPs is the same,  $1.7 \times 10^{11} \text{ cm}^{-2}$  for both substrates. However the covered surface (in %) is larger for the LDPE (65%) compared to SiO<sub>2</sub> (42.6%) due to large eccentricity of AgNPs (the evolution from spherical to prolate spheroid is stronger) when deposited on

polymer substrate. Given the polymer nature of the substrate used in this work, BOPP, our reasoning will be based on the data obtained for a single layer of AgNPs deposited on LDPE polymer substrate.

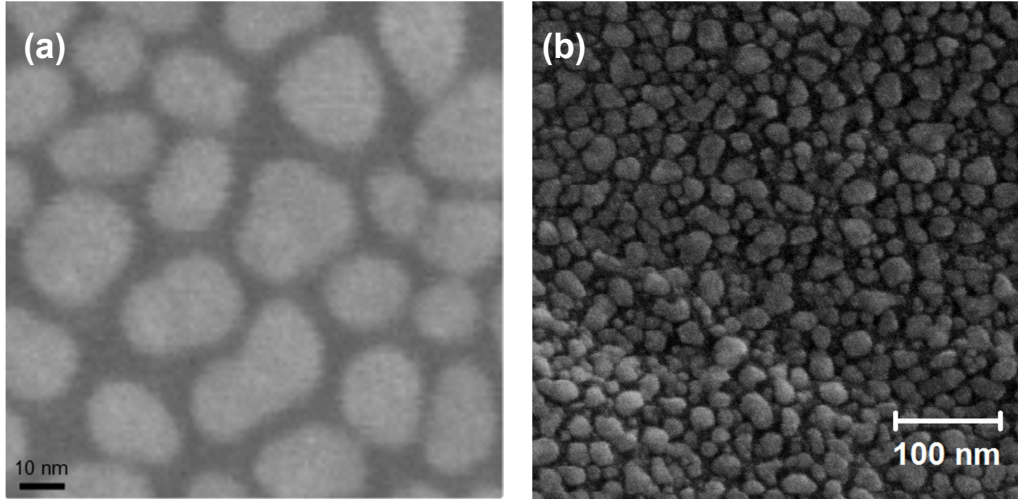


**Figure 3 - 19:**SEM images of a single layer of AgNPs deposited on SiO<sub>2</sub> layer (a) [65] and on LDPE (b) [19].

By varying the plasma parameters one can adapt the multifunctional layer to the target application. The freedom offered by the used plasma process allows for cover layer of either SiO<sub>x</sub>C<sub>y</sub>:H or SiO<sub>2</sub><sup>plasma</sup>, (when adding an opportune amount of oxygen to the plasma gas mixture [46]) including a smooth transition between the two compositions. For our studies we decided to prepare a sample with SiO<sub>x</sub>C<sub>y</sub>:H as cover layer to better adapt to the polymer surface due to the presence of carbon in the layer matrix.

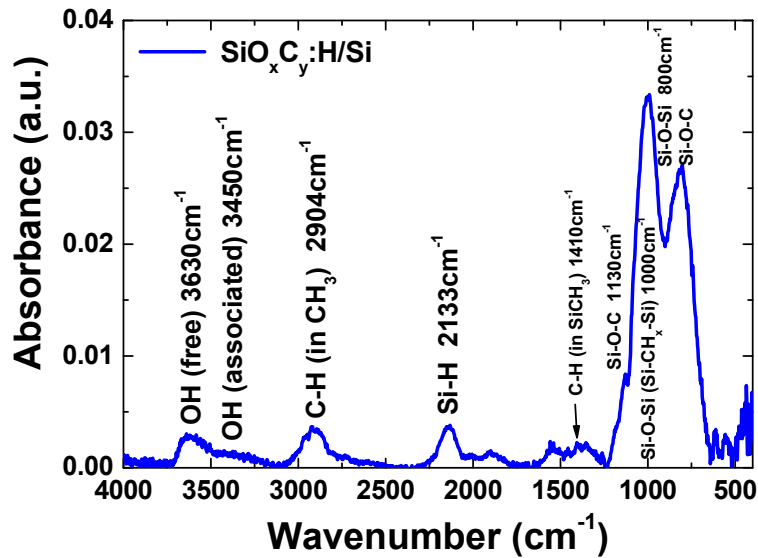


**Figure 3 - 20:** FTIR spectra of plasma deposited organosilicon ( $\text{SiO}_x\text{C}_y\text{:H/Si}$ ) cover layer used in this study [adapted from 51].

As given in Fig. 3-21 the matrix organosilicon layer, observed with Fourier Transform InfraRed (FTIR) spectroscopy, is much less ordered compared to a typical  $\text{SiO}_2$  layer [66]. It presents two broad massifs centred around  $800\text{ cm}^{-1}$  and  $1000\text{ cm}^{-1}$  [51]. The contribution at  $1000\text{ cm}^{-1}$  is ascribed to  $\text{CH}_{x(x<2)}\text{-Si}$  wagging mode. The large pick width approves the amorphous structure of this layer.

Because of the high applied power for sustaining the plasma ( $P = 80\text{ W}$ ), the HMDSO is strongly dissociated which leads to appearance of the asymmetric stretching band Si-H at  $2133\text{ cm}^{-1}$  in the  $\text{SiO}_x\text{C}_y\text{:H}$  layer spectrum. This band is as much intensive as the typically observed C-H asymmetric stretching band in  $\text{CH}_3$  environment at  $2904\text{ cm}^{-1}$ .

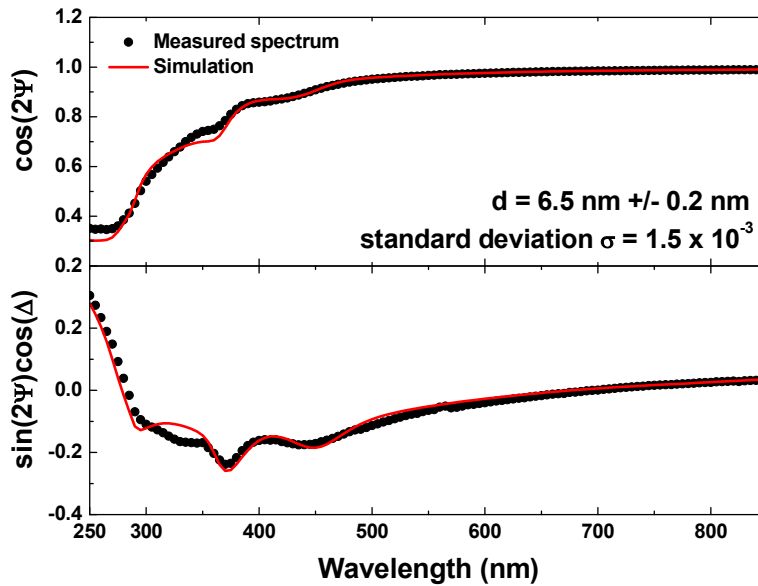


**Figure 3 - 21:** Results for ellipsometric measurements on the organo-silicon cover layer.

To measure the thickness of the organosilicon cover layer by spectroscopic ellipsometry we have added a small Si-substrate during the plasma polymerization step. If we analyse our organosilicon layer at the ellipsometer we achieve the results that we can see in the Figure 3-21. The recorded ellipsometric spectrum was modelled with the Forouhi-Bloomer dispersion law. The layer thickness is controlled by the deposition time and for this layer deposition time of 10 s and gives a layer with thickness of  $6.5 \pm 0.2$  nm.

### 3.2.3 Field dependence of EL under AC stress

#### a) EL-field characteristics

The new BOPP sample with tailored interface was tested under AC stress using the multi-purpose chamber presented in the Chapter 2. In this case, a different protocol was used compared with the first measurements, because the breakdown risk was very high and it was the first time that this kind of sample was tested. It consisted in increasing the voltage by more narrow steps (see later on), up to moderate fields (60, then 90kV/mm), and switching to other type of measurements (as phase resolved EL) without stressing too much the samples. This was

facilitated by the fact that light intensity was much larger than in all previous experiments. In Figure 3-22 we present rough data as EL intensity vs time.

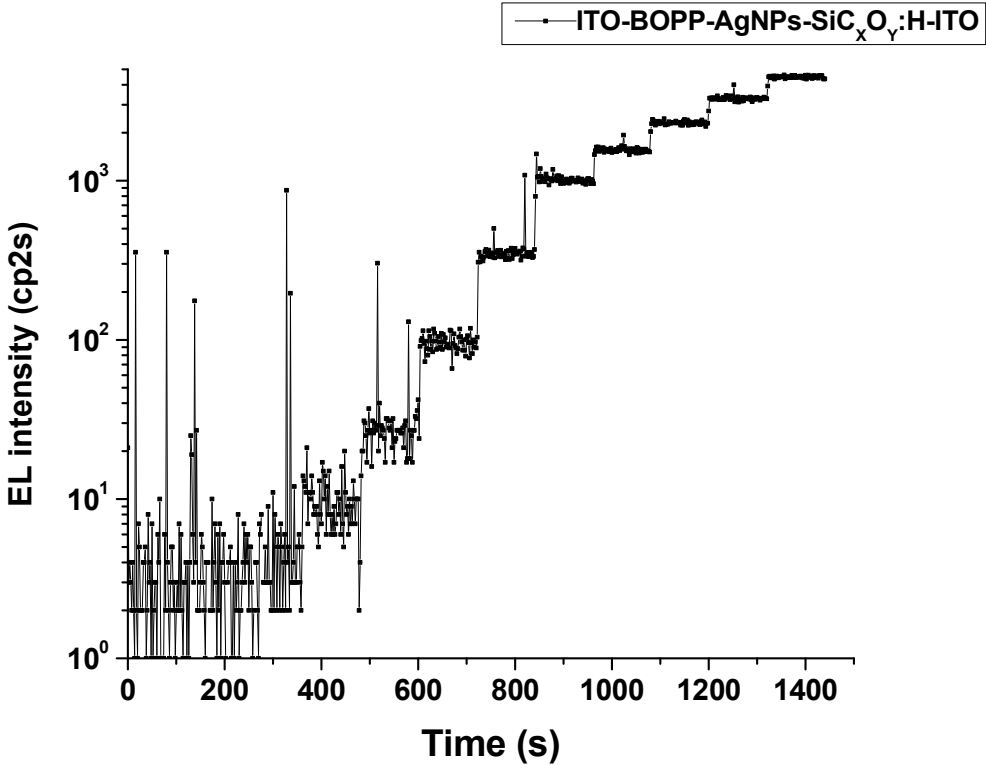


**Figure 3 - 22:** EL intensity vs. time for a multilayer BOPP sample. Light intensity is given in photomultiplier counts per 2 seconds.

If we compare this rough data plot to the data presented in the past section, cf. Fig. 3-3, it is easy to notice that, in this case, the amount of light is substantially higher. Another important difference between the two results is the stability of EL intensity: in the last case presented, even if we are looking at untreated data, we can see a very flat trend of the signal for each step. To elaborate data we used the same procedure as the other sample and we obtain the EL-field characteristic presented in Fig. 3-23.

For this characteristic, the field was increased by step of 5.6 kV/mm between 0 and 11.2 kV/mm and between 67.4 kV/mm and 90 kV/mm and by step of 11.24 kV/mm between 11.2 kV/mm and 67.4 kV/mm. All steps lasted for 120 s.

Looking at the previous measurements, with sample composed by BOPP covered with Au or ITO, it can be seen clearly that the amount of light produced by this new

sample is surprisingly higher. In the Figure 3-24, the characteristics obtained in the three cases are compared. It seems that the characteristic of the sample with AgNPs tailored interface doesn't present the bump immediately after light appearance at low field (up to 40 kV/mm), typical of the Au-BOPP-Au sample. This could mean a lower contribution from the SP in the EL emission, but to clarify this point it is necessary to comment on other type of measurements, like phase resolved EL and spectra.

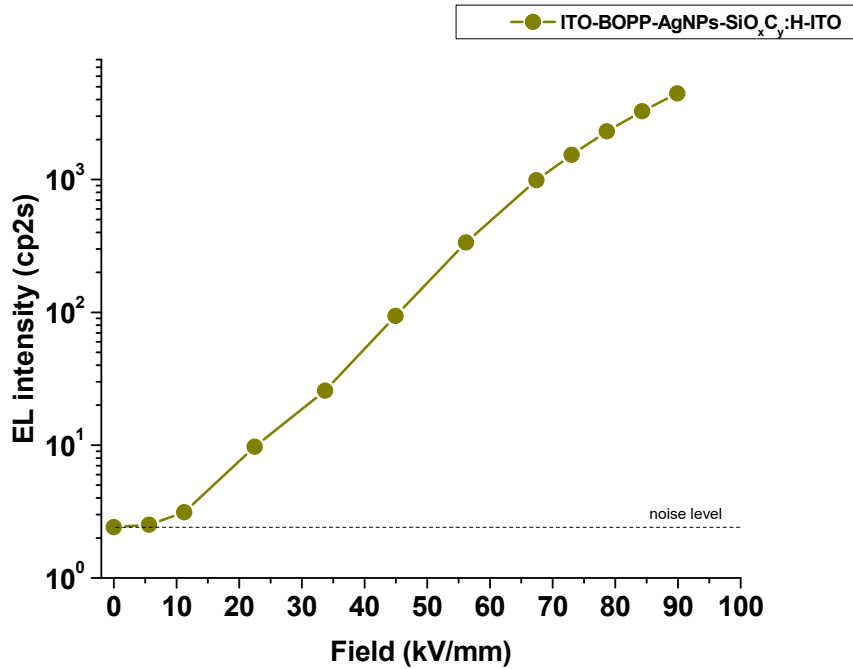


**Figure 3 - 23:** Electroluminescence vs. field of a ITO-BOPP-AgNPs-SiO<sub>x</sub>C<sub>y</sub>:H-ITO sample. The dotted line is EL noise level. “cp2s” stands for counts per 2 s.

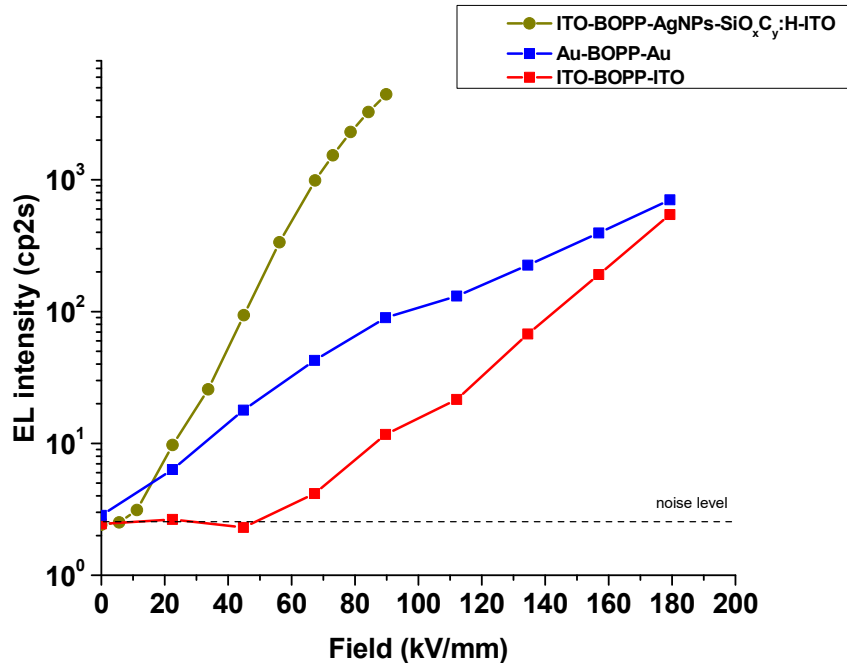


**Figure 3 – 24:** Comparison between EL intensity vs Field for different types of sample. “cp2s” stands for counts for 2 s. The dotted line is the EL noise level.

From Figures 3-23 and 3-24, we can estimate the field threshold for light emission in case of tailored sample to about 10 kV/mm. The light intensity at 90 kV/mm is increased by about 2 decades compared to that for Au-metallized sample.

In the course of the measurements, we noticed a particular behaviour of the AgNPs tailored sample: during the first measure the voltage was increased by step of 5.62 kV/mm lasting 120 s between 0 and 28.1 kV/mm and by step of 11.24 kV/mm between 28.1 and 56.18 kV/mm, obtaining ~800 counts per 2 seconds, an enormous amount of light compared to the previous measurements. Three sequences for voltage increase were used defined as follows and the resulting data are plotted in Figure 3.25:

- sequence 1: From 0 to 56 kV/mm (with changing step as shown in the figure);
- sequence 2: From 35 to 68 kV/mm;
- sequence 3: from 0 to 90 kV/mm (as previously described).

All steps were for 2 minutes, but in-between sequences phase patterns were acquired (not exceeding the maximum field reached in previous sequence). The signal was much stronger compared to previous results, being > ~800 counts per 2 seconds at 56.18 kV/mm.

The noteworthy fact is that with the following measurements at the field of 56.18 kV/mm (sequence 2), the intensity has decreased by a factor of about 2. In the 3<sup>rd</sup> sequence the intensity has further decreased.

In the Figure, we can see the drop of signal between the first sequence and the last one for the same field 56.18 kV/mm, from ~800 counts to ~350 counts.

The explanation for this behaviour is still unknown, to better understand what actually happened to our sample during the measurements it will require more experimental tests with different samples. We just mention this feature for future investigations.

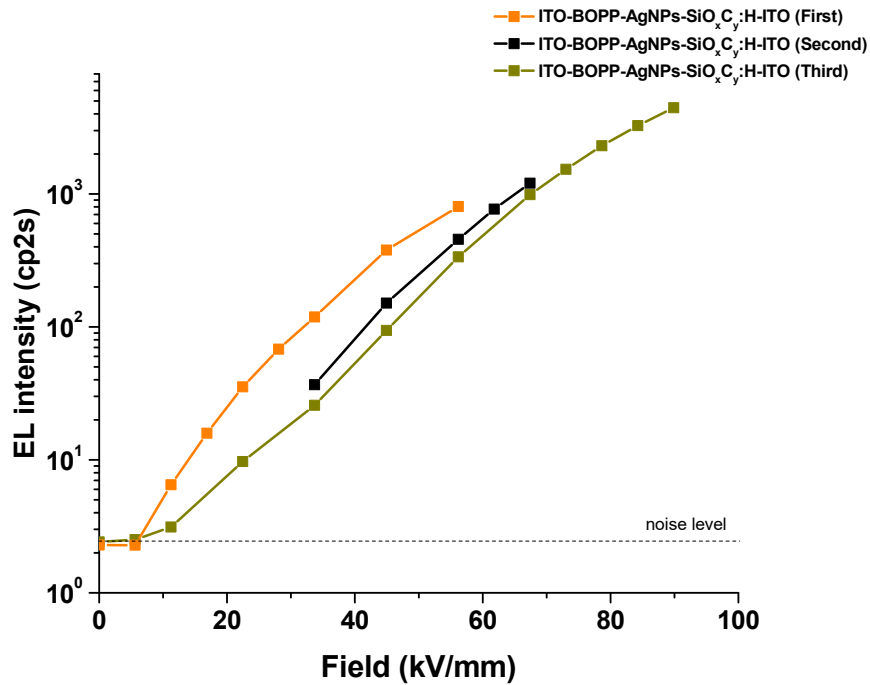


**Figure 3 - 25:** Comparison between EL intensity-Field measurements on the ITO-BOPP-AgNPs-SiO<sub>x</sub>C<sub>y</sub>:H-ITO sample following the 3 sequences in stress.

### **b) Phase resolved EL under AC stress**

Interpretation of the EL dependence on voltage waveform can give us information on charge injection and extraction as well as transport and recombination.

Phase-resolved EL measurements were realized here exactly in the same conditions as in section 3.1: resolution of the phase in 200 data points in one cycle under AC voltage waveform, and an integration time of 2 seconds per memory channel. Various acquisitions were done after each of the sequences described above. As there was no qualitative change in the response, we reported herein only on the full set of patterns obtained after the last sequence (where field was increase up to 90 kV/mm). The noise level is the same as in the other measurements and it is negligible for these measuring conditions under AC.

The field-dependence of phase resolved EL is shown in Figure 3-26 for the same multilayer sample. There exists an advance of EL crest comparing to the voltage crest. However, the advance of phase does not vary with the applied field. It is of about  $19.8^\circ$  and  $28.8^\circ$  for positive and negative half cycles respectively, irrespective of the field. With the previous samples (especially BOPP covered by Gold) the advance decreased with the increment of the field and this behaviour could be related to the Surface Plasmons effect. . It seems that this could be another evidence of a less involvement of Surface Plasmons Effect in the EL emission.

Another notable fact, considering Figure 3-26, is the difference of EL intensity between the two crests. This can be due to the difference between the two surfaces of our sample, in this case, unlike with ITO-BOPP-ITO or Au-BOPP-Au, we don't have a symmetrical electrodes arrangement. The voltage waveform shown in the Figure represents the potential applied to the top electrode, which is the tailored face of the sample. We have substantially more light emission when the top electrode is at negative polarity, i.e. when electrons are injected.

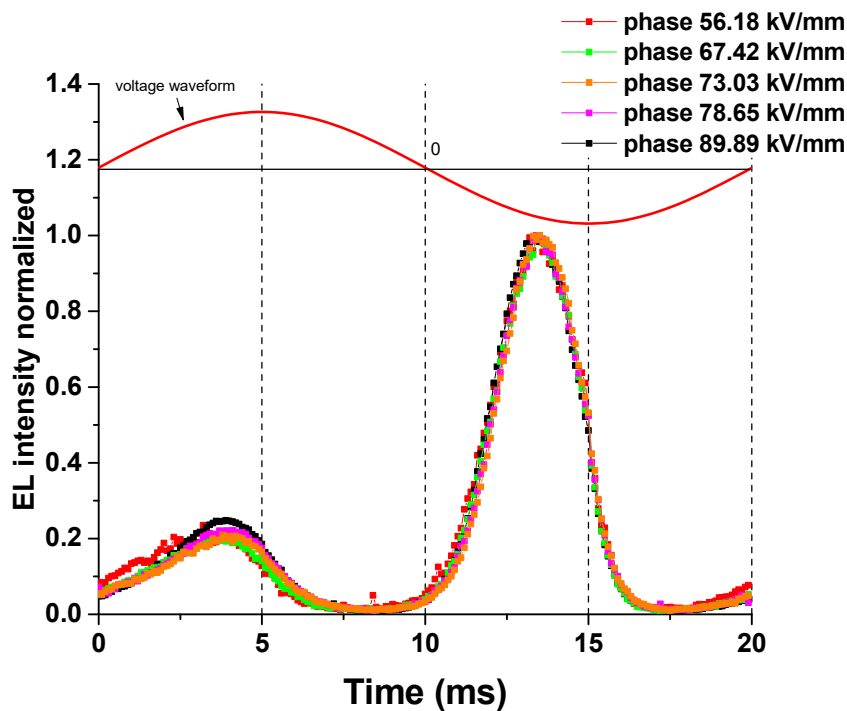


**Figure 3 - 26:** Phase-resolved EL of ITO-BOPP-AgNPs- SiO<sub>x</sub>C<sub>y</sub>:H-ITO sample, under AC sinusoidal stress, measured at uniform frequency 50 Hz under different fields. All the data are normalized at EL wave crest.

### 3.2.4 Spectral analyses

The wavelength-resolved EL spectra under AC stress of the sample with tailored interface are shown in Figure 3-27 in order to identify and analyse the light components. . The integration time with the CCD camera was 180s and the width of the entrance slit placed in front of the grating monochromator was 1 mm. The spectrum is broad and noisy which is due to the low level of EL. It revealed peaks at 415 nm and 573 nm, and shoulders at 505 nm and 650 nm.

The spectral features are better revealed under higher fields due to the increasing light intensity, but the general shape of the spectra does not change: positions of maxima and shoulders are not affected, and there is no extra features revealed under higher field.

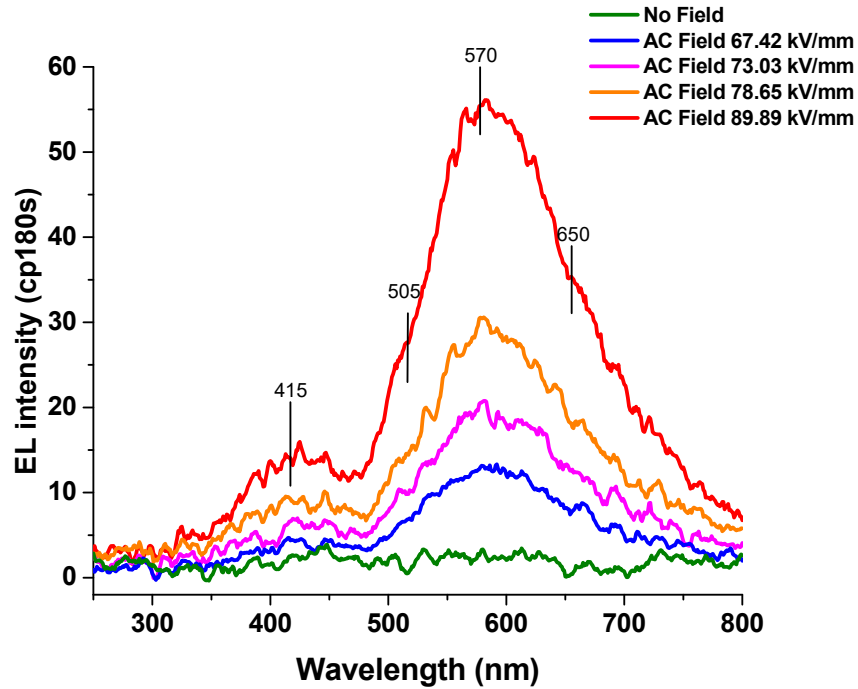


**Figure 3 – 27:** EL spectra of ITO-BOPP-AgNPs- SiO<sub>x</sub>C<sub>y</sub>:H-ITO sample under AC stress.

For the purpose of comparison, we show in Fig. 3.28 the EL spectrum obtained by B Qiao et al. [67] on the same polymer with Au electrodes, and with a larger field (250 kV/mm as crest AC field). The estimated contribution from SP emission corresponds to the spectrum peaking in the red region (maximum at 700-750 nm). The spectrum is compared to that recorded under 5 keV electron beam irradiation, so-called cathodoluminescence –CL- spectrum: it was shown that the CL constitutes a good reproduction of the EL spectrum, with the advantage of much higher light intensity and of avoiding spurious emission as SP contribution. Bands in the CL spectrum were identified at 328, 415, 505 and 573 nm. Most of the bands found in the EL spectrum of BOPP with AgNPs tailored interfaces are present in the CL spectrum. A more detailed analysis is provided below.

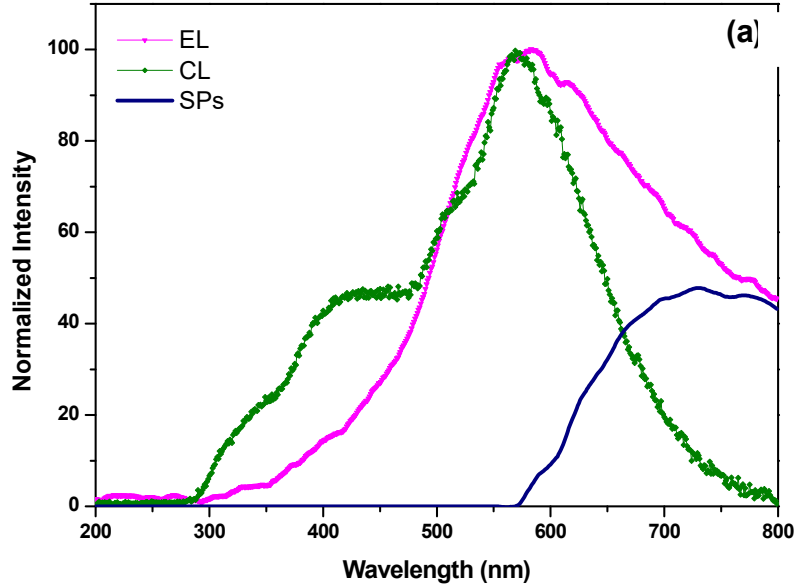


**Figure 3.28:** Electroluminescence spectrum of Au-BOPP-Au sample obtained under a field of 250kV/mm compared to the cathodoluminescence spectrum under 5keV electron beam. The spectrum to the right is the contribution estimate as due to SP emission [67].

### 3.2.5 Discussion

#### a) Spectral reconstruction of EL from BOPP with tailored interface

In the section above, we show that even for the lowest AC field (67kV/mm) were EL spectra were acquired, the EL spectrum appears dominated by emission from PP. In previous work, the EL and CL spectra of BOPP were decomposed into several contributions by curve fitting, the related elementary bands being related to:

- (I) Fluorescence (at 328 nm)
- (II) Chemiluminescence (peak at 415 nm)
- (III) Charge recombination (505 nm)
- (IV) Main band at 570 nm (unknown origin)

Contributions (II) and (IV) dominated in case of EL spectra.

In order to investigate the origin of the peaks in EL spectra of the new multi-layer sample, we propose similar reconstruction of the EL spectrum. For a fitting purpose, the shape of each elementary component has been approximated by a Gauss curve peaking at the same wavelength as the corresponding feature in the

EL spectrum. Multiple peak fitting tool from OriginLab software was used. In this way we can analyse the contribution and the right position of every peak. The reconstructed EL spectrum is shown in Figure 3-29. Contribution from fluorescence was considered insignificant here.

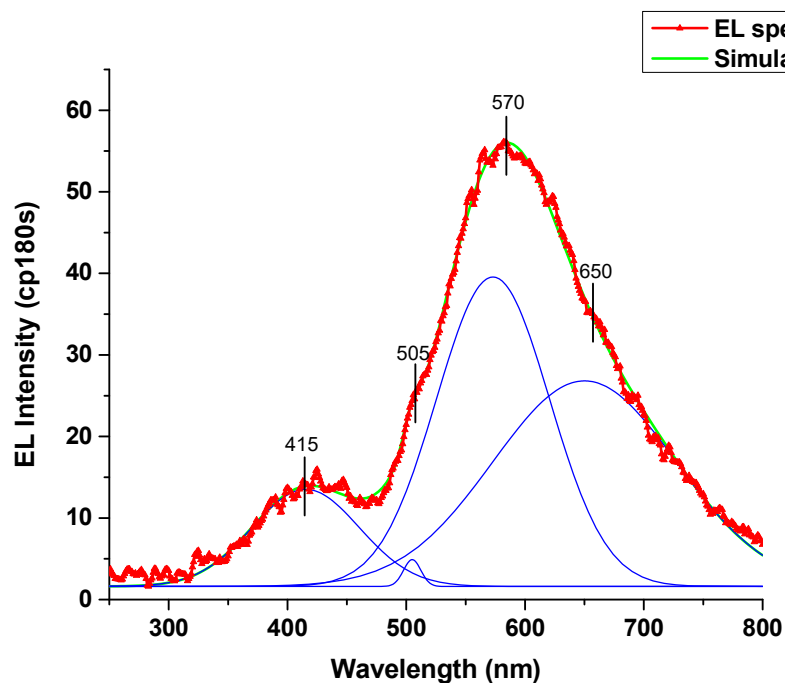


**Figure 3-29:** Reconstruction of EL spectra in ITO-BOPP-AgNPs-SiC<sub>x</sub>O<sub>y</sub>:H-ITO sample. The fit to the experimental data is indicated by the continuous lines.

Fitting the EL spectra by the BOPP EL components could not be done without introducing a peak at higher wavelengths, with maximum around 650 nm. This peak is blue shifted when compared to the emission of SPs on gold as observed on Au/BOPP/Au structures, peaking typically at 750 nm. As this peak is not characteristic of BOPP photo-physical properties (notably it is absent in the cathodoluminescence spectrum), we propose that it corresponds to the SP response of Ag nanoparticles. Its position at 650nm is consistent with reported spectra for Ag emission. As discussed in Chapter 1 the plasmonic properties of Ag appear with much higher amplitude compared to Au and the Au plasmonic peak is systematically observed at higher wavelength, i.e. red-shifted.

## **b) Specific EL feature from BOPP with tailored interfaces**

Comparison of EL features obtained on BOPP with AgNPs tailored interfaces compared to Au or ITO metallized samples are as follows:

- Light is much more intense using AgNPs tailored interface, whether we compare it to ITO or Au-metallized samples.

- The bump in EL field characteristic is not present – or at least not in the same range of field. The characteristic of Fig 3.25 could indeed be interpreted as a kind of bump – data at higher field would be necessary to analyse deeper.

- On sample with AgNPs tailored interface, the phase angle of EL does not depend on field in the investigated field range (50-90kV/mm). In fact angles are close to those obtained with ITO electrodes (see Table 3-1).

- The contribution from SP emission is blue-shifted from 750 nm for Au to 650 nm for AgNPs. In the spectra reported here, the relative contribution from SP radiative emission appears smaller considering AgNPs.

- EL spectra of BOPP with tailored interfaces show all the features of e-beam excited material, notably with contributions from chemiluminescence, showing that energetic carriers might be at play in EL excitation.

The impact of AgNPs on the EL emission from BOPP can be manifold:

- It was shown previously that AgNPs efficiently store electrical charges when used as artificial deep traps [19]. With AC stress, charges of opposite polarity alternatively injected and trapped may create excitation of SPs of AgNPs by the ac field, hence the SP-related emission;

- The fact that charges are trapped on AgNPs in one half period increases the field in the second half period, and hence a larger amount of carriers are injected;

- NPs could act through an increase of the probability of having radiative recombination as reported in some works [68]: the light production yield in BOPP would be increased. This would be consistent with the small penetration length of charges necessary to reproduce EL-phase patterns in modelling. However, amplification effects reported in light emitting diodes are of the order of 20% while we have here an increase by 2 decades.

Further work is necessary to elucidate the detailed mechanisms: the effects shown here can be very useful to understand the EL in polyolefins on the one hand and the photophysical properties of nanoparticles on the other hand.

### **3.3 Conclusion and Perspective**

The thesis was directed to the improvement of understanding of surface plasmon contribution in the electroluminescence processes of an insulating polymer, bioriented polypropylene –BOPP-, along with to investigate, through electroluminescence detection, how the electronic properties of interfaces are modified when introducing a nanocomposite layer containing Ag nanoparticles at the surface of the polymer film. These works constitute a follow up of the theses of L Millière and B Qiao recently defended at Laplace.

In the first part of this experimental work, we repeat some of the measurements obtained by B. Qiao in his thesis, which was focused on a comparison of the EL and cathodoluminescence features of different polymers, mainly BOPP. The present study aimed at a firm confirmation of the observed features and also at pushing further some of the unsolved questions, notably the behaviour of the phase angle of EL depending on electrode nature and experimental conditions.

For this reason I started EL measurements on MIM (metal-insulator-metal) configuration with gold or ITO as electrode. In this case, during EL measurement, I observed that the light intensity of BOPP films under AC stress is relatively high because the alternative voltage produces injection of charges of alternating polarity into the material. The light intensity and the shape of the characteristics may vary from sample to sample, but there is a common feature in that the curves exhibit a typical upward convex shape in the low field region, that can be called “bump” for simplicity. This “bump” has already been reported and studied on different type of gold metallized polymer films under AC stress. This emission has been attributed in previous studies to the relaxation of Surface Plasmons (SPs) excited by charge injection-extraction at the interface between gold electrodes and the dielectric material.

Surface Plasmons excited in metals, as reported in previous studies, can radiate light in the red part of the optical spectrum upon decay. For this reason I repeated the measurements applying an optical filter along the path of the photomultiplier with the intent of suppressing the red component emissions. A supplementary evidence of the involvement of SP was provided by the fact that the “bump” is not detected in this case. So, only the emission characteristic of the insulating material remains. The investigation of the phase of the EL in respect to the AC stress has unambiguously demonstrated that the signal issued from SP emission is clearly more in advance than that issued from bulk PP emission. This constitutes, besides spectra acquisition, a further means to differentiate the two processes at play in EL from insulations.

With the intent to check the SP hypothesis I changed the structure of the sample and this was the core of the second part of the research work. The idea was to deposit a mono layer of AgNPs embedded in an organosilicon (SiOC:H) matrix on one face of the BOPP substrate. Then both sides were covered with an ITO layer to form the final structure under study.

Achieving this kind of structure on a thin polymeric material has been a hard work because of its high sensitivity to temperature. In fact, the BOPP has a thickness of 17.8  $\mu\text{m}$  and processes like plasma deposition can easily damage it.

After the realisation of this new sample with AgNPs, I tested it in the same multi-purpose chamber as for the previous samples for different field and I obtained some striking results. As I reported in the previous section of this thesis, the amount of light produced by this new sample is surprisingly higher, up to two orders of magnitude in the investigated field range up to 90kV/mm, compared with samples composed by BOPP covered with Au or ITO.

To better understand the origin of this surprisingly amount of light I recorded (measured) the spectra of the light produced by the new type of sample during EL measurements and I noticed that the SP contribution is blue-shifted in comparison with that of the BOPP sample covered with Au. In fact the peak attributed to SPs with Au was localised at 750 nm and in the sample with AgNPs was at 650 nm, meaning at lower wavelength, higher energy. This behaviour is consistent with the relative position of absorption bands of the two metals in the UV-vis region. Independently from the plasmon contribution, the EL from modified samples has BOPP-related emissions intensity much higher than with simple Au or ITO

electrodes. A possible explanation to the behaviour is the increase of the probability of having radiative recombination due to the presence of silver NPs.

In this dissertation we reported a very interesting effect that can be very useful to understand the EL emission in polymeric material as BOPP, the photophysical properties of nanoparticles and the interactions between these kinds of materials. Further work is necessary to elucidate the detailed mechanism. For example it could be very interesting to compare the EL response considering different electrodes: Au vs. Ag continuous electrodes. So far much work has been done with Au but Ag has been seldom considered.

Secondly, the impact of the size of AgNPs particles is to be investigated as their plasmonic features are dependent on the size of grains (changing from bulk metal properties to NPs and to Ag clusters). Also, the distance of the particles from the surface can be tuned by acting on the SiOCH layer thickness. A further way to act on plasmonic phenomena is to change the dielectric substrate with changing its permittivity: optical properties of the particles are changed accordingly.

The above actions are likely to bring new understanding of phenomena at play with attempting to distinguish the role of particles with electromagnetic waves confinement, the role of electrical charges (tunnelling injection, charging of particles and of the material, recombination with charges of opposite carriers), and the nature of excited states into the polymer substrate, their excitation mechanism, and the depth of the active layer. These questions are present in the literature on semiconductors with incorporation of metallic NPs, very attractive phenomena are observed, but the hypotheses are many and the processes not yet thoroughly understood.

# References

- [1] J. Wisniak, "Jons Jacob Berzelius, A Guide to the Perplexed Chemist", *The Chem. Educ.*, 5(6):343-350, 2000
- [2] A. Rudin, "The Elements of Polymer Science and Engineering", Academic Press, 1982
- [3] I. Pleša, P. V. Nojtingher, S. Schlögl, C. Sumereder, M. Muhr, "Properties of Polymer Composites Used in High-Voltage Applications", *Polymers* 2016, 8, 173.
- [4] C. K. Chiang, C. R. Fincher, Y. W. Park, A. J. Heeger, H. Shirakawa, E. J. Louis, et al., "Electrical conductivity in doped polyacetylene," *Phys. Rev. Lett.*, vol. 39, pp. 1098-1101, 1977.
- [5] R. H. Friend, R. W. Gymer, A. B. Holmes, J. H. Burroughes, R. N. Marks, C. Taliani, et al., "Electroluminescence in conjugated polymers," *Nature*, vol. 397, pp. 121-128, 1999.
- [6] U. Mitschke and P. Bauerle, "The electroluminescence of organic materials," *J. Mater. Chem.*, vol. 10, pp. 1471-1507, 2000.
- [7] G. Teyssedre and C. Laurent, "Advances in high-field insulating polymeric materials over the past 50 years," *IEEE Electr. Insul. Mag.*, vol. 29, pp. 26-36, 2013.
- [8] K. N. Mathes, "A Brief History of Development in Electrical Insulation", *Electrical Electronics Insulation Conference, 1991. Boston '91 EEIC/ICWA Exposition, Proceedings of the 20<sup>th</sup>.*
- [9] A. Haque, M. Shamsuzzoha and F. Hussain, "S2- Glass/Epoxy Polymer Nanocomposites: Manufacturing, structure, thermal and mechanical properties", *J. Comp. Mats.*, 2003, pp. 1821-1837.
- [10] F. L. Matthews, R. D. Rawlings, "In Composite Materials: Engineering and Science", 2nd ed.; CRC Press, Woodhead Publishing Limited: Cambridge, UK, 1999; pp. 1–28.
- [11] J. K. Nelson, "Overview of Nano dielectrics: Insulating materials of the future". In *Proceedings of the Electrical Insulation Conference and Electrical Manufacturing Expo, Nashville, TN, USA, 22–24 October 2007*; pp. 229–235.
- [12] T. Tanaka, G.C. Montanari, R. Mülhaupt, "Polymer nanocomposites as dielectrics and electrical insulation, Perspectives for processing technologies, material characterization and future applications". *IEEE Trans. Dielectr. Electr. Insul.* 2004, 11, pp. 763–784.
- [13] G. Chen, J. Zhao, S. Li, L. Zhong, "Origin of thickness dependent dc electrical breakdown in dielectrics", *Appl. Phys. Lett.*, Vol. 100, p. 222904, 2012.
- [14] Y. Zhang, J. Lewiner, C. Alquié, N. Hampton, "Evidence of strong correlation between space-charge buildup and breakdown in cable insulation", *IEEE Trans. Dielectr. Insul.*, Vol. 3, pp. 778-783, 1996.
- [15] L.A. Dissado, G. Mazzanti and G.C. Montanari, "The incorporation of space charge degradation in the life model for electrical insulating materials", *IEEE Trans. Dielectr. Electr. Insul.*, Vol. 2, pp. 1147-1158, 1995.
- [16] G.C. Montanari, "Bringing an insulation to failure: the role of space charge", *IEEE Trans. Dielectr. Electr. Insul.*, Vol. 18, pp. 339-364, 2011.

- [17] C. Laurent, G. Teyssède, S. Le Roy and F. Baudoin, "Charge dynamics and its energetic features, in polymeric materials", *IEEE Trans. Dielectr. Electr. Insul*, Vol. 20, pp. 357-381, 2013.
- [18] L. Milliere, K. Makasheva, C. Laurent, B. Despax, and G. Teyssedre. Efficient barrier for charge injection in polyethylene by silver nanoparticles/plasma polymer stack, *Appl. Phys. Lett.*, **105**, 122908(5pp), 2014.
- [19] L. Milliere, K. Makasheva, C. Laurent, B. Despax, L. Boudou, and G. Teyssedre. "Silver nanoparticles as a key feature of a plasma polymer composite layer in mitigation of charge injection into polyethylene under dc stress", *J. Phys. D: Appl. Phys.*, **49**, 015304(13pp), 2016.
- [20] L. Millière. "Maîtrise des interfaces pour le contrôle de l'injection de charges dans les polymères isolants électriques", PhD dissertation, Toulouse University, France, 2015.
- [21] C. Laurent, G. Teyssedre, J.L. Auge, F. Mazzanti, G. C. Montanari, L. A. Dissado, J. Fothergill, A. Seeley, "Space charge and associated electroluminescence processes in XLPE cable peelings", 2000, 69th Annual Conference on Electrical Insulation and Dielectric Phenomena.
- [22] C. Laurent, F. Massines, C. Mayoux, "Optical emission due to space charge effects in electrically stressed polymers", *IEEE Trans. on DEI*, Vol. 4, N°6, pp. 585-603, October 1997.
- [23] G. Teyssedre, G. Tardieu, D. Mary, and C. Laurent, "Ac and dc electroluminescence in insulating polymers and implication for electrical ageing," *J. Phys. D: Appl. Phys.*, vol. 34, pp. 2220-2229, 2001
- [24] H. Reather, "Surface plasmons on smooth and rough surfaces and on gratings", Springer-Verlag, Vol. 111, 1988.
- [25] S. Nie, S. R. Emory. Probing Single Molecules and Single Nanoparticles by Surface-Enhanced Raman Scattering, *Science*, 1997, 275, 1102-1106.
- [26] J. Toudert, D. Babonneau, L. Simonot, S. Camelio, T. Girardeau. Quantitative modelling of the surface plasmon resonances of metal nanoclusters sandwiched between dielectric layers: the influence of nanocluster size, shape and organization, *Nanotechnology*, 2008, 19, 125709.
- [27] A. Traverse, C. Humbert, C. Six, A. Gayral, B. Busson. Nonlinear optical properties of Ag nanoparticles embedded in Si<sub>3</sub>N<sub>4</sub>, *EPL*, 2008, **83**, 64004.
- [28] G. Baffou, R. Quidant. Thermo-plasmonics: using metallic nanostructures as nano-sources of heat, *Laser Photonics Rev.*, 2013, 7, 171-187.
- [29] H. A. Atwater, A. Polman. Plasmonics for improved photovoltaic devices, *Nat. Mater*, 2010, 9, 205-213.
- [30] S. Linic, P. Christopher, D. B. Ingram. Plasmonic-metal nanostructures for efficient conversion of solar to chemical energy, *Nat. Mater*, 2011, **10**, 911-921.
- [31] B. Despax, C. Saulou, P. Raynaud, L. Datas and M. Mercier-Bonin, "Transmission electron microscopy for elucidating the impact of silver-based treatments (ionic silver versus nanosilver-containing coating) on the model yeast *Saccharomyces cerevisiae*", *Nanotechnology* **22**, 175101, 2011.

- [32] A. Pugliara, K. Makasheva, B. Despax, M. Bayle, R. Carles, P. Benzo, G. BenAssayag, B. Pécassou, M.-C. Sancho, E. Navarro, Y. Echegoyen, and C. Bonafos, "Assessing bio-available silver released from silver nanoparticles embedded in silica layers using the green algae *Chlamydomonas reinhardtii* as bio-sensors," *Journal Science of the Total Environment*, **565**, 863-871, 2016.
- [33] P. Spinelli, A. Polman. "Prospects of near-field plasmonic absorption enhancement in semiconductor materials using embedded Ag nanoparticles", *Opt. Express*, 2012, 20, A641-A654.
- [34] S. C. Warren, D. A. Walker, B. A. Grzybowski, "Plasmoelectronics: Coupling Plasmonic Excitation with Electron Flow", *Langmuir*, 2012, **28**, 9093-9102.
- [35] G. Prieto, J. Zečević, H. Friedrich, K. P. De Jong, P. E. De Jongh. Towards stable catalysts by controlling collective properties of supported metal nanoparticles, *Nat. Mater*, 2013, **12**, 34-39.
- [36] S. Mukherjee, F. Libisch, N. Large, O. Neumann, L. V. Brown, J. Cheng, J. B. Lassiter, E. A. Carter, P. Nordlander, N. J. Halas. Hot Electrons Do the Impossible: Plasmon-Induced Dissociation of H<sub>2</sub> on Au, *Nano Lett.*, 2013, 13, 240-247.
- [37] J. Z. Zhang. Optical properties and spectroscopy of nanomaterials, 2009, World Sci. Pub., London.
- [38] A. Pugliara, "Elaboration of nanocomposites based on Ag nanoparticles embedded in dielectrics for controlled bactericide properties", PhD dissertation, Toulouse University, France, 2016.
- [39] M. Bayle, 'Architectures plasmoniques enterrées : élaboration, propriétés optiques et applications', PhD dissertation, Toulouse University, France, 2014.
- [40] M. A. Lieberman and A. J. Lichtenberg, Principle of Plasma Discharges and Materials Processing, Hoboken, New Jersey: John Wiley & Sons, Inc., 2005.
- [41] E. Kay and M. Hecq, "Metal clusters in plasma polymerized matrices: Gold", *J. Appl. Phys.*, 1984, 55, 340-374.
- [42] F. Massines, P. Segur, N. Gherardi, C. Khamphan, A. Ricard, "Physics and chemistry in a glow dielectric barrier discharge at atmospheric pressure: diagnostics and modelling", *Surface and Coatings Technology*, 2003, 174-175, 8-14.
- [43] B. Despax, P. Raynaud, "Deposition of "Polysiloxane" Thin Films Containing Silver Particles by an RF Asymmetrical Discharge", *Plasma Process. Polym.*, 2007, 4, 127-134.
- [44] U. Kortshagen, "Non-thermal plasma synthesis of semiconductor nanocrystals", *J. Phys. D: Appl. Phys.*, 2009, 42, 113001.
- [45] T. Belmonte, G. Arnoult, G. Henrion, T. Gries, "Nanoscience with non-equilibrium plasmas at atmospheric pressure", *Environ. J. Phys. D: Appl. Phys.*, 2011, 44, 363001.
- [46] A. Pugliara, C. Bonafos, R. Carles, B. Despax, K. Makasheva, "Controlled elaboration of large-area plasmonic substrates by plasma process", *Materials Research Express* 2, 065005, 2015.
- [47] M. Soumbo, A. Pugliara, A. Mlayah, M.-C. Monje, C. Roques, B. Despax, C. Bonafos, R. Carles, and K. Makasheva. On the application of Surface Enhanced Raman Scattering to study the interaction of DsRed fluorescent proteins with silver nanoparticles embedded

in thin silica layers, *Book Series IEEE Nanotechnology Materials and Devices Conference (IEEE NMDC 2016)*, **1**, 104(2pp), 2016.

[48] J.P. Jones, J.P. Llewellyn, and T.J. Lewis, "The contribution of field induced morphological change to the electrical aging and breakdown of polyethylene", *IEEE Trans. Dielect. Electr. Insul.*, vol. 12, pp. 951-966, 2005.

[49] S. Delpino, D. Fabiani, G.C. Montanari, C. Laurent, G. Teyssedre, P.H.F. Morshuis, R. Bodega, and L.A. Dissado, "Polymeric HVDC cable design and space charge accumulation. Part 2: insulation interfaces", *IEEE Electr. Insul. Mag.*, vol. 24, No. 1, pp. 14-24, 2008.

[50] T. T. N. Vu, G. Teyssedre, B. Vissouvanadin, S. Le Roy, and C. Laurent, "Correlating Conductivity and Space Charge Measurements in Multi-dielectrics under Various Electrical and Thermal Stresses," *IEEE Trans. Dielect. Electr. Insul.*, vol. 22, pp. 117-127, 2015.

[51] K. Makasheva, C. Villeneuve-Faure, C. Bonafos, C. Laurent, A. Pugliara, B. Despax, L. Boudou, and G. Teyssedre, 'Dielectric Engineering of Nanostructured Layers to Control the Transport of Injected Charges in Thin Dielectrics', *IEEE Trans. Nanotechnology*, **15**, 839-848, 2016.

[52] A. T. Jones, J. M. Aizlewood, and D. Beckett, "Crystalline forms of isotactic polypropylene," *Die Makromolekulare Chemie*, vol. 75, pp. 134-158, 1964.

[53] S. Boggs, Private Communication, 2014.

[54] B. Qiao "Electrical ageing of insulating polymers: approach through electroluminescence and cathodoluminescence analyses," PhD dissertation, Toulouse University, France, 2015.

[55] V. M. Donnelly, "Optical diagnostic techniques for low pressure plasma processing", in *Plasma-Surface Interactions and Processing of Materials*, NATO ASI Series vol. 176, pp. 57-93, 1990.

[56] F. Bernoux, J.-P. Piel, B. Castellon, C. Defranoux, J.-H. Lecat, P. Boher, J.-L. Stehlé. 'Ellipsométrie - Théorie, *Techniques de l'ingénieur*', 2003, R6490 V1.

[57] B. Qiao, C. Laurent, G. Teyssedre, "Evidence of Exciton Formation in Thin Polypropylene Films under AC and DC Fields and Relationship to Electrical Degradation", *IEEJ Trans. Fundamentals and Materials* 136, 74-80, 2016

[58] S. Tamura, K. Ohta, and T. Kanai, "Study of crater structure formation on the surface of biaxially oriented polypropylene film," *J. Appl. Polym. Sci.*, vol. 124, pp. 2725-2735, 2012.

[59] S. Tamura and T. Kanai, "Control of well-defined crater structures on the surface of biaxially oriented polypropylene film by adding nucleators," *J. Appl. Polym. Sci.*, vol. 130, pp. 3555-3564, 2013.

[60] L. Cisse, G. Teyssedre, D. Mary, C. Laurent. "Influence of voltage frequency, the electrode material and a superimposed dc bias on ac electroluminescence of polymer films" *IEEE Trans. Dielect. Electr. Insul.* 9, pp. 124-129, 2002

[61] F. Baudoin, D. H. Mills, P. L. Lewin, S. Le Roy, G. Teyssedre, and C. Laurent, "Modeling electroluminescence in insulating polymers under ac stress: effect of excitation waveform," *J. Phys. D: Appl. Phys.*, vol. 44, p. 165402, 2011.

- [62] F. Baudoin, D. H. Mills, P. L. Lewin, S. Le Roy, G. Teyssedre, C. Laurent, et al., "Modelling electroluminescence in insulating polymers under ac stress: effect of voltage offset and pre-stressing," *J. Phys. D: Appl. Phys.*, vol. 45, p. 325303, 2012.
- [63] C. Laurent and C. Mayoux, "Light detection during the initiation of electrical treeing at room temperature," *J. Phys. D: Appl. Phys.*, vol. 14, pp. 1903-1910, 1981.
- [64] T. Tanaka and A. Greenwood, "Effects of charge injection and extraction on tree initiation in polyethylene," *IEEE Transactions on Power Apparatus and Systems*, vol. PAS-97, pp. 1749-1759, 1978.
- [65] A. Pugliara, K. Makasheva, B. Despax, M. Bayle, R. Carles, P. Benzo, G. BenAssayag, B. Pécassou, and C. Bonafos, "Optical response of delta-layer of silver nanoparticles embedded near the free surface of thin silica matrix," *Workshop "Nanomatériaux, nano-objets pour la détection et les capteurs"*, RTRA STAE, December 2–4, 2013, Nailloux, France.
- [66] C. T. Kirk, "Quantitative analysis of the effect of disorder-induced mode coupling on infrared absorption in silica," *Phys. Rev. B*, **38**, 1255–1273, 1988.
- [67] B. Qiao, C. Laurent, G. Teyssedre, "Electroluminescence and cathodoluminescence from polyethylene and polypropylene films: spectra reconstruction from elementary components and underlying mechanisms", *J. Appl. Phys.* **119**, 024103-01/11, 2016
- [68] B. Munkhbat, H. Pöhl, P. Denk, T. Klar, M. Scharber, C. Hrelescu, "Performance Boost of Organic Light-Emitting Diodes with Plasmonic Nanostars", *Advanced Optical Materials* **4**, 772-781, 2016.